Nanosecond to Microsecond Protein Dynamics Probed by Magnetic Relaxation Dispersion of Buried Water Molecules

Erik Persson and Bertil Halle*

Department of Biophysical Chemistry, Center for Molecular Protein Science, Lund University, SE-22100 Lund, Sweden

Received October 2, 2007; E-mail: bertil.halle@bpc.lu.se

Abstract: Large-scale protein conformational motions on nanosecond−microsecond time scales are important for many biological processes, but remain largely unexplored because of methodological limitations. NMR relaxation methods can access these time scales if protein tumbling is prevented, but the isotropy required for high-resolution solution NMR is then lost. However, if the immobilized protein molecules are randomly oriented, the water ^2H and ^{17}O spins relax as in a solution of freely tumbling protein molecules, with the crucial difference that they now sample motions on all time scales up to $\sim 100\ \mu$s. In particular, the exchange rates of internal water molecules can be determined directly from the ^2H or ^{17}O magnetic relaxation dispersion (MRD) profile. This possibility opens up a new window for characterizing the motions of individual internal water molecules as well as the large-scale protein conformational fluctuations that govern the exchange rates of structural water molecules. We introduce and validate this new NMR method by presenting and analyzing an extensive set of ^2H and ^{17}O MRD data from cross-linked gels of two model proteins: bovine pancreatic trypsin inhibitor and ubiquitin. We determine residence times and order parameters of four internal water molecules in these proteins and show that they are quantitatively consistent with the information available from crystallography and solution MRD. We also show how slow motions of side-chains bearing labile hydrogens can be monitored by the same approach. Proteins of any size can be studied at physiological hydration levels with this method.

1. Introduction

Native proteins adopt unique three-dimensional structures, but their biological functions usually rely on structural flexibility. The relative positions of protein atoms undergo thermal fluctuations under the influence of interactions within the protein and with the solvent. Because of the complexity of the underlying free energy landscape, the internal dynamics of proteins span a wide range of time scales: from subpicosecond bond librations to microsecond dihedral jumps and much slower domain movements and partial unfolding events. Such motions are essential for molecular recognition, binding, gating, signal transduction, transport, and chemical transformation in all living systems.

To characterize the full repertoire of internal protein dynamics is a more challenging task than to determine the mean protein structure, because no single experimental technique can probe the wide range of time scales involved. While the structural database is approaching completeness (with respect to new folds), our knowledge of protein dynamics is still highly fragmented. Much of the available information about protein dynamics has come from methods that exploit nuclear spin relaxation phenomena.[1] In a protein solution, all anisotropic nuclear spin couplings (e.g., magnetic dipole−dipole, magnetic shielding anisotropy, electric quadrupole) are averaged to zero by protein tumbling, so the spin relaxation induced by these couplings cannot report on internal motions slower than the protein tumbling time of, typically, several nanoseconds.[2] Much slower motions, from tens of microseconds and into the millisecond range, can be detected via their effects on the isotropic chemical shift.[3] But this still leaves a significant time scale gap, $10^{-8}-10^{-5}$ s, that cannot be probed directly by solution NMR relaxation techniques and that is not yet accessible by conventional molecular dynamics simulations.[4]

If protein rotation can be inhibited, a wider range of time scales becomes accessible by nuclear spin relaxation. This is the case in protein (micro-)crystals and precipitates, which are increasingly being studied with solid-state NMR techniques.[5] While this is a promising development, there is a risk that direct protein−protein contacts not only inhibit protein rotation but also perturb the internal motions under study. Furthermore, crucial system variables like pH and temperature are difficult to control in such experiments. A different approach, where the protein remains fully hydrated, measures residual dipolar couplings from a protein dissolved in an aligned medium.[6] This method can give information about the angular amplitude of internal motions slower than protein tumbling, but it cannot furnish the rates (or correlation times) of these motions.

(1) Mittermaier, A.; Kay, L. E. *Science* **2006**, *312*, 224−228.

(2) Jarymowycz, V. A.; Stone, M. J. *Chem. Rev.* **2006**, *106*, 1624−1671.
(3) Palmer, A. G.; Massi, F. *Chem. Rev.* **2006**, *106*, 1700−1719.
(4) Adcock, S. A.; McCammon, J. A. *Chem. Rev.* **2006**, *106*, 1589−1615.
(5) Krushelnitsky, A.; Reichert, D. *Progr. NMR Spectrosc.* **2005**, *47*, 1−25.
(6) Lakomek, N. A.; Carlomagno, T.; Becker, S.; Griesinger, C.; Meiler, J. *J. Biomol. NMR* **2006**, *34*, 101−115.

Here, we present and apply a new nuclear spin relaxation approach that provides access to internal protein motions on the elusive time scale $10^{-8}-10^{-5}$ s. In this approach, the protein is immobilized by chemical crosslinking,[7] rather than by direct protein−protein contacts. The resulting gel contains >90% water, so the protein is fully hydrated. Because protein tumbling is inhibited, slower internal motions can be studied via spin relaxation induced by anisotropic nuclear couplings, but not via the protein resonances, which are too broad to be studied by solution NMR. (Also solid-state NMR is inapplicable, since the dilute gel would be damaged by fast sample spinning.) Instead, we monitor protein dynamics via relaxation effects on the water ^2H and ^{17}O resonances, conveyed by internal water molecules. Nearly all proteins have one or more water molecules buried in internal cavities, providing structural stability by satisfying the H-bond capacity of the peptide backbone.[8,9] Such internal water molecules are conserved to the same extent as the amino acid sequence[10] and may thus be regarded as the 21st amino acid.

A typical internal water molecule is strongly coupled to the protein structure, being linked to it by three or four strong H-bonds. As long as it remains inside the protein, the water molecule is thus orientationally restrained. But once the water molecule escapes from the cavity, its orientation is randomized on a picosecond time scale by molecular rotation in the external solvent. We monitor this process via the quadrupolar relaxation of water ^2H and ^{17}O nuclei, which, in contrast to nonexchanging protein nuclei, experience an isotropic system. In aqueous biopolymer gels, the exchange-mediated orientational randomization (EMOR) of internal water molecules is the dominant relaxation mechanism at low Larmor frequencies.[11−13] By recording the Larmor frequency dependence of the spin−lattice relaxation rate, the so-called magnetic relaxation dispersion (MRD), over as much as 5 orders of magnitude in frequency, we can directly determine the residence times of individual water molecules at crystallographically identified internal sites. Because internal water exchange is gated by conformational fluctuations in the protein,[14] these residence times report on internal protein dynamics on a wide range of time scales.

Because internal water molecules exchange with external solvent, they cannot be detected directly by solution NMR. In high-resolution NOE studies of protein solutions, internal water molecules are detected indirectly via cross-relaxation with protein protons.[15] Provided that magnetization transfer pathways via chemical exchange of nearby labile protein protons can be excluded, intermolecular water−protein NOEs provide an approximate lower bound of ∼0.5 ns on the residence time.[16] In solution MRD studies, internal water molecules are detected indirectly via their relaxation effect, which is proportional to

the tumbling time of the protein.[17,18] When the protein is immobilized, the relaxation effect depends instead on the internal water residence time, which usually is much longer than the tumbling time of the free protein. The sensitivity of the MRD technique is thereby greatly enhanced. MRD studies of freely tumbling proteins can usually only provide collective lower and upper bounds on the residence times of all rapidly exchanging internal water molecules in a protein.[17,18] In contrast, when the protein is immobilized, the actual residence times can be accurately determined for the individual internal water molecules. The power of the EMOR/MRD approach is illustrated here by determining the residence times of four internal water molecules in bovine pancreatic trypsin inhibitor (BPTI) and ubiquitin, thus providing new insights into the slow conformational dynamics of these proteins.

Although it is applicable to proteins of arbitrary size, the EMOR/MRD approach will here be demonstrated and validated on two small proteins, BPTI and ubiquitin. These proteins have long served as testing ground for novel NMR techniques and their internal water molecules have been studied in greater detail than for any other proteins. BPTI contains four internal water molecules[19−22] (Figure 1) in a deep grove between two extensive loops that mediate the exceptionally strong inhibitory binding of BPTI to β-trypsin.[22] One water molecule, labeled W122 in the crystal structure 5PTI,[19] is buried in a tight-fitting cavity near the 14−38 disulfide bond, where it engages in four, nearly tetrahedrally arranged, H-bonds with backbone peptide atoms. The remaining three internal water molecules, W111−W113, form a H-bonded water chain that penetrates a narrow pore with a small opening near the disordered Glu7 side-chain.[19,20] These four water molecules are involved in 11 H-bonds with the protein, bridging the binding loop backbones in four places and thus contributing to the rigidity that is believed to be essential for the inhibitory function of BPTI.[22] The residence time of W122, 0.4 ms at 20 °C, happens to be in a range where it could be determined from temperature-dependent solution MRD data.[14] The residence times of W111−W113 have not been determined, but solution MRD studies have confined them to the range $10^{-8}-10^{-5}$ s.[23,24] If the 14−38 disulfide bond is disrupted, also W122 exchanges on this time scale.[25]

Ubiquitin was originally chosen as a model protein in MRD studies because it has no deeply buried water molecules, but the MRD data indicate that one water molecule has a residence time longer than 10 ns.[23] The only likely candidate is W28, buried in a superficial cavity or deep pocket, depending on how the protein surface is defined (Figure 1). Present in all crystal

(7) Migneault, I.; Dartiguenave, C.; Bertrand, M. J.; Waldron, K. C. *Biotechniques* **2004**, *37*, 790−802.

(8) Williams, M. A.; Goodfellow, J. M.; Thornton, J. M. *Protein Sci.* **1994**, *3*, 1224−1235.

(9) Park, S.; Saven, J. G. *Proteins* **2005**, *60*, 450−463.

(10) Baker, E. N. In *Protein-Solvent Interactions*; Gregory, R. B., Ed.; M. Dekker: New York, 1995; pp 143−189.

(11) Halle, B. *Progr. NMR Spectrosc.* **1996**, *28*, 137−159.

(12) Vaca Chávez, F.; Persson, E.; Halle, B. *J. Am. Chem. Soc.* **2006**, *128*, 4902−4910.

(13) Vaca Chávez, F.; Hellstrand, E.; Halle, B. *J. Phys. Chem. B* **2006**, *110*, 21551−21559.

(14) Denisov, V. P.; Peters, J.; Hörlein, H. D.; Halle, B. *Nat. Struct. Biol.* **1996**, *3*, 505−509.

(15) Otting, G.; Wüthrich, K. *J. Am. Chem. Soc.* **1989**, *111*, 1871−1875.

(16) Otting, G. *Progr. NMR Spectrosc.* **1997**, *31*, 259−285.

(17) Halle, B.; Denisov, V. P.; Venu, K. In *Biological Magnetic Resonance*; Krishna, N. R., Berliner, L. J., Eds.; Kluwer/Plenum: New York 1999; pp 419−484.

(18) Halle, B. In *Hydration Processes in Biology*; Bellisent-Funel, M.-C., Ed.; IOS Press: Dordrecht, The Netherlands, 1998; pp 233−249.

(19) Wlodawer, A.; Walter, J.; Huber, R.; Sjölin, L. *J. Mol. Biol.* **1984**, *180*, 301−329.

(20) Parkin, S., Rupp, B., and Hope, H. *Acta Crystallogr. D* **1996**, *52*, 18−29.

(21) Addlagatta, A.; Krzywda, S.; Czapinska, H.; Otlewski, J.; Jaskolski, M. *Acta Crystallogr. D* **2001**, *57*, 649−663.

(22) Hanson, W. M.; Domek, G. J.; Horvarth, M. P.; Goldenberg, D. P. *J. Mol. Biol.* **2007**, *366*, 230−243.

(23) Denisov, V. P.; Halle, B. *J. Mol. Biol.* **1995**, *245*, 682−697.

(24) Denisov, V. P.; Halle, B.; Peters, J.; Hörlein, H. D. *Biochemistry* **1995**, *34*, 9046−9051.

(25) Denisov, V. P.; Peters, J.; Hörlein, H. D.; Halle, B. *Biochemistry* **2004**, *43*, 12020−12027.
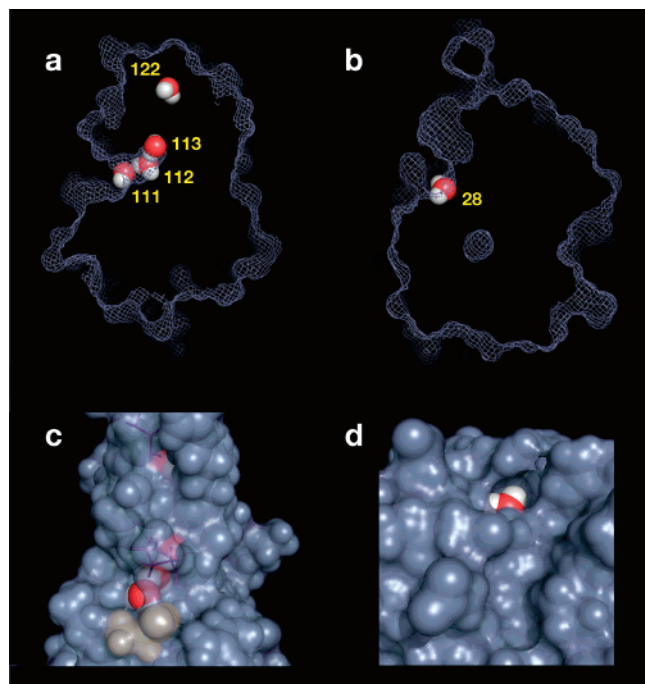
Figure 1. Internal water molecules in BPTI (a, c) and ubiquitin (b, d). Panels a and b show slices through the protein molecules, revealing water burial depth and connectivity with external solvent, while panels b, and d emphasize surface topography and atomic packing. The images are based on the room-temperature crystal structures 5PTI[19] (BPTI) and 1UBQ[26] (ubiquitin, H atoms added). They were rendered with PyMOL,[29] using 1.2 Å probe radius to define the (external and internal) molecular surfaces of the proteins and with all atomic radii reduced by 10%. In panel c, the Pro13 and Lys41 side chains of BPTI are shown in stick representation to make all four internal water molecules visible through the semitransparent molecular surface. The Glu7 side chain is in the closed (A) conformation in panel c (yellow-colored atoms) and the open (B) conformation in panel a.

structures of ubiquitin, W28 makes two strong H-bonds with backbone atoms.[26−28]

2. Materials and Methods

2.1. Sample Preparation. Bovine pancreatic trypsin inhibitor (BPTI, trade name Trasylol, batch 9104, 97% purity by HPLC) was obtained from Bayer HealthCare AG (Wuppertal, Germany). To remove residual salt, the protein was exhaustively dialyzed against Millipore water (Millipore, Billerica, MA) and lyophilized. Ubiquitin was expressed in *E. coli* and purified to >99% (see Supporting Information). Lyophilized protein was dissolved in D_2O or in $H_2^{17}O$. The pH was adjusted by microliter additions of HCl or NaOH followed by centrifugation. The protein concentration of the solution (before crosslinking) was determined by complete amino acid analysis. The protein was then crosslinked by addition of ice-cold 25% glutaraldehyde (GA) solution as detailed in the Supporting Information. Table 1 shows the composition and pH of all gels examined by ^2H or ^{17}O MRD. The protein and GA concentrations are specified as the water/protein mole ratio, N_W, and the GA/protein mole ratio, N_{GA}.

The bifunctional crosslinking reagent GA has been used widely for protein immobilization.[7] GA reacts primarily with Lys (and N-terminal) amino groups, forming stable cross-links by a mechanism that has not been firmly established.[7] The GA/Lys stoichiometry of the reaction is reported[30] to be ∼4 and N_{GA} was chosen to allow essentially all amino

Table 1. Composition of Protein Gels Studied by ^2H or ^{17}O MRD.

label	protein	solvent	pH/pD	N_W	N_{GA}
B1	BPTI	$H_2^{17}O$	4.1	3285	26
B2	BPTI	D_2O	6.5	3259	29
B3	BPTI	D_2O	4.4	3615	32
B4	BPTI	D_2O	4.5	2317	32
B5	BPTI	D_2O	4.3	2709	55
U1	ubiquitin	$H_2^{17}O$	4.9	3806	23
U2	ubiquitin	D_2O	5.3	2812	26

groups in BPTI (5) and ubiquitin (8) to participate in cross-links. The amino groups are fairly uniformly distributed over the protein surfaces.

2.2. Magnetic Relaxation Dispersion. The water-^2H longitudinal relaxation rate, R_1, was measured from 1.5 kHz to 92 MHz using six different NMR spectrometers, including a fast field-cycling instrument, a variable-field iron-core magnet, and four superconducting magnets. The longitudinal (R_1) and transverse (R_2) relaxation rates of the water ^{17}O magnetization were measured over 2.5 frequency decades, using Tecmag spectrometers equipped with iron-core magnets. The sample temperature was maintained at 27.0 ± 0.1 °C. Single-exponential recovery/decay curves were obtained throughout and fits to the MRD data were made with the Levenberg−Marquardt nonlinear least-squares algorithm with equal weighting of all data points. Further details about the MRD experiments are provided in Supporting Information.

To facilitate comparison of MRD data from different BPTI gel samples, all relaxation rates have been normalized to $N_W = 3000$, using the fact that $R_1 - R_{1,bulk}$ is inversely proportional to N_W (see eq 1 and Figure S1).

3. Theoretical Basis of the EMOR/MRD Method

3.1. Mobile versus Immobilized Proteins. The relaxation rate, R_1, of the longitudinal water ^2H or ^{17}O magnetization probes the rotational dynamics of individual water molecules via rotationally induced fluctuations of the nuclear electric quadrupole coupling.[31] The rate of molecular rotation—or its inverse, the rotational correlation time, $τ_R$—can be determined directly from the dependence of R_1 on the nuclear Larmor frequency, $ν_0$, in the frequency range where $ω_0 ≡ 2πν_0$ is of the order $1/τ_R$. For the ^2H and ^{17}O nuclides, the highest attainable Larmor frequency is ∼0.1 GHz, so only correlation times $τ_R > 1$ ns can be determined directly from the MRD profile, $R_1(ω_0)$.

In bulk water at room temperature, $τ_R ≈ 2$ ps so $R_{1,bulk}$ is independent of $ω_0$. The motions of the majority of the water molecules interacting with the external protein surface are somewhat slower, but not so much as to render R_1 frequency dependent.[32] For a water molecule residing in a small polar cavity inside a protein, the H-bond polarity imposed by the surrounding protein atoms effectively prevents water rotation and only allows small-amplitude librations and symmetric 180° flips about the water dipole axis. Because these motions are strongly anisotropic, they do not average out the nuclear quadrupole coupling.[17] Furthermore, they are either too fast (librations) or too infrequent (C_2 flips) to contribute significantly to spin relaxation. In protein solutions, the residual quadrupole coupling of internal water molecules that remains after partial orientational averaging by librations and C_2 flips is averaged to zero by the rotational diffusion of the protein carrying the

(26) Vijay-Kumar, S.; Bugg, C. E.; Cook, W. J. *J. Mol. Biol.* **1987**, *194*, 531−544.

(27) Alexeev, D.; Bury, S. M.; Turner, M. A.; Ogunjobi, O. M.; Muir, T. W.; Ramage, R.; Sawyer, L. *Biochem. J.* **1994**, *299*, 159−163.

(28) Bang, D.; Makhatadze, G. I.; Tereshko, V.; Kossiakoff, A. A.; Kent, S. B. *Angew. Chem., Int. Ed.* **2005**, *44*, 3852−3856.

(29) DeLano, W. L. The PyMOL Molecular Graphics System (2002). http://www.pymol.org.

(30) Korn, A. H.; Feairheller, S. H.; Filachione, E. M. *J. Mol. Biol.* **1972**, *65*, 525−529.

(31) Abragam, A. *The Principles of Nuclear Magnetism*; Clarendon Press: Oxford, U.K., 1961.

(32) Halle, B. *Phil. Trans. R. Soc. London, Ser. B* **2004**, *359*, 1207−1224.

orientationally restrained internal water molecules. This is usually the only significant source of relaxation dispersion. The correlation time extracted from the MRD profile from a protein solution is thus the rotational correlation time of the freely tumbling protein, τ_{RP}, typically 5−10 ns.

In isotropic solutions, protein tumbling completely randomizes the orientation of internal water molecules. The MRD profile, $R_1(\omega_0)$, is therefore flat at Larmor frequencies $\omega_0 \ll 1/\tau_{RP}$ and does not provide any information about dynamic processes on time scales longer than τ_{RP}. This limitation can be removed by immobilizing the protein, as in the chemically crosslinked protein gels investigated here. Because protein rotation is now inhibited, the residual nuclear quadrupole coupling is averaged to zero by the exchange of orientationally restrained internal water molecules with rapidly rotating bulk-like water. We refer to this mechanism as exchange-mediated orientational randomization (EMOR).[11−13] The exchange rate— or its inverse, the mean residence time, τ_W—of individual internal water molecules can thus be determined in a direct and essentially model-independent way from the MRD profile. The long-time limit is now set by the inverse nuclear quadrupole frequency rather than by the protein tumbling time, so the range of accessible correlation times is increased from 1 order of magnitude (1−10 ns) for a small protein in solution to 4 orders of magnitude (10 ns−100 μs for ^{2}H) for an immobilized protein (of any size).

To probe these slow motions, the relaxation rate must be measured at very low Larmor frequencies. For the ^{2}H nuclide, we measure R_1 down to 1.5 kHz (corresponding to a magnetic field strength of 0.2 mT) with the field-cycling technique.[33,34] For ^{17}O, which relaxes too rapidly for field-cycling to be used, the signal-to-noise deterioration at low fields sets the low-frequency limit to ∼0.5 MHz.

3.2. Spin Relaxation Theory. The MRD profile from immobilized proteins cannot be fully analyzed with the conventional Bloch−Wangsness−Redfield (BWR) perturbation theory of nuclear spin relaxation, which requires the randomizing motion to be fast compared to the nuclear quadrupole frequency, ω_Q.[31] BWR theory is thus a useful approximation only for internal water molecules with residence times shorter than ∼1 μs (^{2}H) or ∼0.15 μs (^{17}O). The MRD profiles from immobilized proteins tend to be dominated by internal water molecules with residence times near these limits (if present). The quantitative analysis of MRD data then requires a more general (nonperturbative) relaxation theory, based on stochastic Liouville theory (SLT).[11] Fortunately, the MRD profile can still be obtained in analytical form, or with modest computational effort, in the dilute regime, where internal water molecules are greatly outnumbered by bulk water molecules.

The MRD data reported here were analyzed with the theoretical expression

$$R_1(\omega_0) = (1 - f_S - f_I) R_{1,\text{bulk}} + f_S R_{1,S}(\omega_0) + \sum_k f_k R_{1,k}(\omega_0) \quad (1)$$

where $f_k = N_k / N_W$ is the fraction of water molecules in the kth internal site, $f_I = \Sigma_k f_k$, and $f_S = N_S / N_W$ is the fraction water molecules that experience a significant dynamic perturbation due to interactions with external protein surfaces. Equation 1

has the same *form* as the BWR expression for fast exchange among several water sites or environments,[17] but it is actually valid without restrictions on the exchange time (which is also the correlation time in the EMOR mechanism), provided that the system is in the dilute regime ($f_k \ll 1$ or $N_W \gg 1$) and that the apparent intrinsic relaxation rate, $R_{1,k}$, in site k is treated by SLT.[11−13]

For internal water molecules relaxed by the EMOR mechanism, the intrinsic relaxation rate in the dilute regime can be expressed as[11−13]

$$R_{1,k}(\omega_0) = \bar{\omega}_{Q,k}^2 \tau_k F_I(L_k, Q_k, \bar{\eta}_k) \quad (2)$$

where τ_k is the mean residence time of the internal water molecule in site k. The residual nuclear quadrupole frequency $\bar{\omega}_{Q,k}$, defined as in previous solution MRD studies,[17] is partially averaged by restricted rotational motions in site k on time scales shorter than τ_k. This may be formalized by writing

$$\bar{\omega}_{Q,k} = \omega_Q^0 S_k \quad (3)$$

where $\omega_Q^0 = 8.7 \times 10^5$ s^{-1} (^{2}H) or 7.6×10^6 s^{-1} (^{17}O) is the rigid-lattice (corrected for librational averaging) quadrupole frequency of water molecules in hexagonal ice.[17] Internal water molecules usually engage in three or four H-bonds so the electric field gradient should differ little from that in ice. If the field gradient is the same as in ice, the quantity S_k may be interpreted as a rank-2 orientational order parameter, ranging from 0 (isotropic orientational averaging) to 1 (no orientational averaging). However, because the field gradient may differ slightly from the ice value, we regard S_k as an apparent order parameter which may (slightly) exceed 1.

The function $F_I(L_k, Q_k, \bar{\eta}_k)$ in eq 2 has three dimensionless arguments. The motionally induced asymmetry parameter $\bar{\eta}_k$, ranging from 0 to 1, measures the deviation from axial symmetry of the residual electric field gradient tensor at the (^{2}H or ^{17}O) nuclear site,[31] induced by motions on time scales shorter than τ_k. This quantity is distinct from the rigid-lattice asymmetry parameter, η_0, which is incorporated as $(1 + \eta_0^2/3)^{1/2}$ in the quadrupole frequency, ω_Q^0.[17] If an internal water molecule is rigidly attached to the protein and if the protein is rigidly fixed in the gel network, then $S_k = 1$ (if $\omega_{Q,k} = \omega_Q^0$) and $\bar{\eta}_k = \eta_0$. For ^{2}H, the rigid-lattice asymmetry parameter, $\eta_0 = 0.1$. Extensively H-bonded internal water molecules are known to be highly ordered,[14,35] so if the protein is also highly immobilized we expect the order parameter, S_k, to be large and, for ^{2}H, the asymmetry parameter, $\bar{\eta}_k$, to be small. Conversely, for ^{2}H, a $\bar{\eta}_k$ value close to 1 is not compatible with a large S_k value.

The reduced Larmor frequency is $L_k \equiv \omega_0 \tau_k$ and the reduced nuclear quadrupole frequency is defined as

$$Q_k \equiv \left(\frac{\alpha_I}{1 + \bar{\eta}_k^2/3} \right)^{1/2} \bar{\omega}_{Q,k} \tau_k \quad (4)$$

The spin-dependent numerical factor α_I equals 3/2 for ^{2}H (spin, $I = 1$) and 15/16 for ^{17}O ($I = 5/2$). The SLT result in eq 2 is exact for any values of the dimensionless quantities L_k and Q_k. In particular, it is valid for arbitrary long residence time, τ_k. In general, the spin-dependent function $F_I(L_k, Q_k, \bar{\eta}_k)$ must be

(33) Noack, F. *Progr. NMR Spectrosc.* **1986**, *18*, 171−276.
(34) Ferrante, G.; Sykora, S. *Adv. Inorg. Chem.* **2005**, *57*, 405−470.

(35) Denisov, V. P.; Venu, K.; Peters, J.; Hörlein, H. D.; Halle, B. *J. Phys. Chem. B* **1997**, *101*, 9380−9389.
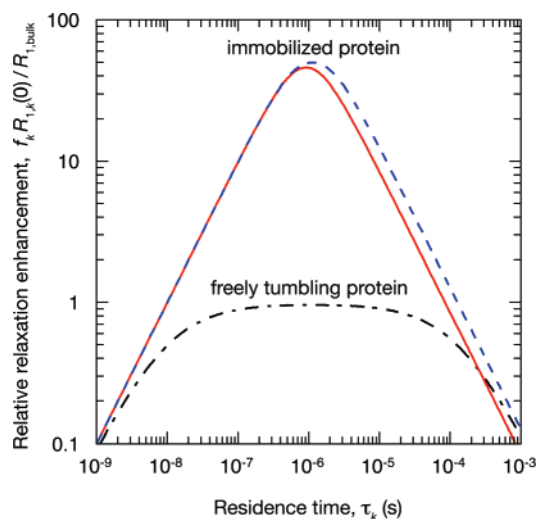
Figure 2. Relative ^{2}H relaxation enhancement at zero frequency from a single internal water molecule with residence time τ_k (and $S_k = 1$) against a background of 3000 bulk water molecules (with $R_{1,\text{bulk}} = 2.6$ s^{-1}). The solid and dashed curves refer to an immobilized protein with $\bar{\eta}_k = 0$ or 1, respectively. For comparison, the dash−dotted curve shows the corresponding relaxation enhancement for a freely tumbling protein with $\tau_{RP} = 10$ ns.

computed numerically as an orientational average over certain supermatrix elements.[11] Rather than reproducing the lengthy exact expressions used in the analysis of the ^{2}H MRD data, we indicate the general structure of the function by giving an approximate analytical result (T. Nilsson and B. Halle, to be published) which coincides with the exact result everywhere in the $L_k - Q_k$ plane, except for the small region where $Q_k \approx L_k > 1$. For ^{2}H ($I = 1$), the approximate result is

$$F_1(L_k,Q_k,\bar{\eta}_k) = \frac{1}{2}\left(1 + \frac{\bar{\eta}_k^2}{3}\right)^{-1} \sum_{n=0,\pm} A_n\left[\frac{0.2}{1 + A_nQ_k^2 + L_k^2} + \frac{0.8}{1 + A_nQ_k^2 + 4L_k^2}\right] \quad (5)$$

where

$$A_0 = \frac{4}{9}\bar{\eta}_k^2, \quad A_\pm = \left(1 \pm \frac{\bar{\eta}_k}{3}\right)^2 \quad (6)$$

In the BWR regime of short residence times, defined as $Q_k^2 \ll 1 + L_k^2$, this more general result reduces to the familiar[31] expression

$$F_1(L_k,Q_k,\bar{\eta}_k) = \frac{0.2}{1 + L_k^2} + \frac{0.8}{1 + 4L_k^2} \quad (7)$$

MRD is among the few methods that can detect individual internal water molecules in a protein solution with a vast excess (up to 10^5-fold) of bulk water. In *solution*, this is possible because a water molecule buried in a protein with a typical tumbling time of 10 ns, rotates 5000-fold slower than a water molecule in the bulk solvent. This difference is manifested directly in the relaxation rate at frequencies below the MHz dispersion, because $R_{1,k}(0)$ is proportional to the correlation time. For an *immobilized* protein, the dynamic weighting is even more pronounced because the correlation time is now the residence time, which can be much longer than the tumbling time of the free protein. In the example shown in Figure 2, a single internal

water molecule with 1 μs residence time in the presence of a 3000-fold excess of bulk water enhances the low-frequency relaxation rate, $R_1(0)$, by a factor 50, whereas only a doubling of $R_1(0)$ is obtained in the solution case. Since R_1 can be measured with 1−2% accuracy over the whole frequency range, an enhancement of $R_1(0)$ by 10% of $R_{1,\text{bulk}}$ can easily be measured. Therefore, as seen from Figure 2, ^{2}H MRD can detect individual internal water molecules with residence times in the range 10 ns−100 μs. If a protein contains one or more internal water molecules with $\tau_k \approx 1$ μs, then they will dominate $R_1(0)$ and it will be more difficult to simultaneously detect other internal water molecules with much shorter or much longer residence times (Figure 2).

The general shape of the curves for immobilized proteins in Figure 2 follows directly from the theory. In the case $\bar{\eta}_k = 0$, eq 5 (which is exact at $\omega_0 = 0$) yields with eq 2:

$$R_{1,k}(0) = \frac{\bar{\omega}_{Q,k}^2 \tau_k}{1 + \alpha_I(\bar{\omega}_{Q,k}\tau_k)^2} \quad (8)$$

Thus, for residence times shorter than $1/\bar{\omega}_{Q,k} \approx 1$ μs, the relaxation enhancement increases linearly with τ_k, whereas, for residence times longer than $1/\bar{\omega}_{Q,k}$, the relaxation enhancement is proportional to $1/\tau_k$.

Because of the larger quadrupole frequency, $\bar{\omega}_{Q,k}$, the ^{17}O nuclide cannot detect the most long-lived internal water molecules that can be seen by ^{2}H MRD. For the proteins studied here, the internal water molecules that contribute significantly to the ^{17}O MRD profile have residence times on the short-τ_k side of the maximum in Figure 2, where the dependence on the asymmetry parameter, $\bar{\eta}_k$, is negligibly weak. We therefore analyze the ^{17}O data with the following analytical approximation to the exact $\bar{\eta}_k = 0$ result (T. Nilsson and B. Halle, to be published):

$$F_{5/2}(L_k,Q_k,0) = \frac{2}{7}\left[\frac{0.2}{1 + Q_k^2 + L_k^2} + \frac{0.8}{1 + Q_k^2 + 4L_k^2}\right] + \frac{5}{7}$$
$$\left[\frac{0.2}{1 + 4Q_k^2 + L_k^2} + \frac{0.8}{1 + 4Q_k^2 + 4L_k^2}\right] \quad (9)$$

with Q_k defined by eq 4. In the BWR limit, $Q_k^2 \ll 1 + L_k^2$, this expression reduces to eq 7.

4. Results and Discussion

4.1. BPTI : ^{2}H MRD Profile. Figure 3 shows water ^{2}H and ^{17}O MRD profiles from immobilized BPTI. All MRD profiles presented here exhibit a high-frequency dispersion component with a correlation time of a few nanoseconds. This universal contribution, which we attribute to external hydration, is analyzed in section 4.7. Here, we focus instead on the low-frequency components that directly reflect exchange of internal water molecules via the EMOR mechanism (section 3). As shown in section 4.3, labile BPTI deuterons do not contribute significantly to R_1 at pD 6.5 (sample B2, used for the measurements in Figure 3a).

The residence time of the singly buried W122 (Figure 1) has previously[14] been determined by ^{2}H and ^{17}O solution MRD: $\tau_{W122} = 0.4$ ms in D$_2$O solution at 20 °C. Since $\bar{\omega}_{Q,W122}\tau_{W122} \gg 1$, the contribution of W122 to R_1 is negligibly small. Indeed, from eqs 1 and 8, this contribution can be estimated as $2f_{W122}/(3\tau_{W122}) \approx 0.6$ s^{-1}. For ^{17}O, the corresponding estimate is 0.4
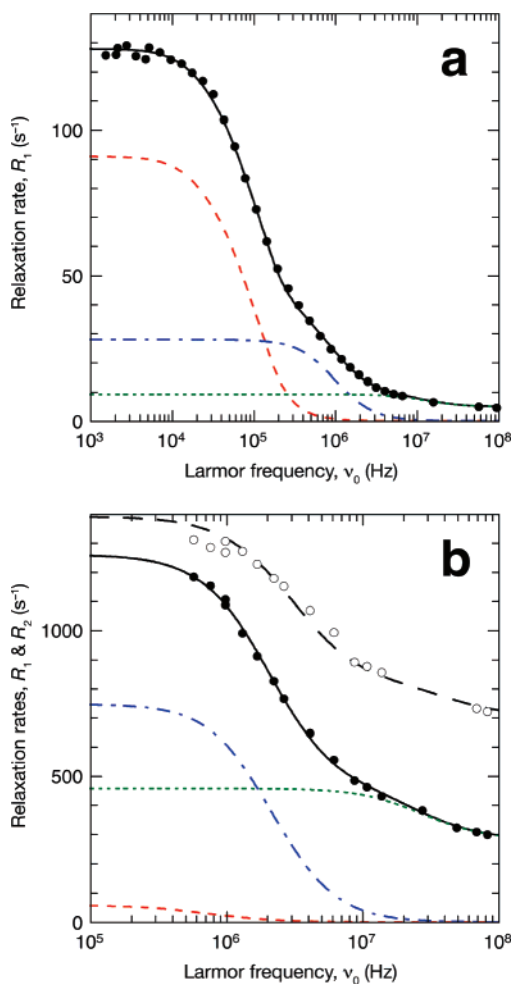
Figure 3. Water ^{2}H (a) and ^{17}O (b) MRD profiles from immobilized BPTI at 20 °C. The data were measured on samples B2 (a) and B1 (b) and are normalized to $N_W = 3000$. Filled and open circles represent R_1 and R_2 data, respectively. The solid curves were obtained by fitting the model to the R_1 data as described in the text. The broken curves are the contributions to R_1 from internal water molecules W112 and W113 (red) and W111 (blue) and from bulk and surface hydration water (green). The parameter values resulting from the fits are given in Table 2. In panel b, the dashed R_2 profile was computed from the parameters obtained from the R_1 fit.

s^{-1}. We can thus safely neglect the contribution of W122 to the ^{2}H and ^{17}O MRD profiles. The low-frequency dispersions observed with immobilized BPTI (Figure 3) must therefore be produced by the mutually H-bonded chain of internal water molecules, W111, W112, and W113 (Figure 1).

If these three internal water molecules have residence times in the range 10^{-8}–10^{-5} s, as indicated by previous solution MRD studies,[23,24] and if the three residence times are sufficiently different from each other, then the ^{2}H MRD profile in Figure 3a should reveal three distinct (albeit overlapping) EMOR components. However, a fit with three EMOR components yields an unphysically large asymmetry parameter, $\bar{\eta}_k \approx 1$, for the slowest component (section 3). We therefore reject this scenario and proceed on the assumption that two of the three residence times are so close that they are not resolved by our data.

A fit with two EMOR components yields one residence time ($k = 1$) of several μs and another one ($k = 2$) on the order of 0.1 μs (Table 2). These two components can be assigned to the three water molecules in two ways: either $N_1 = 1$ and $N_2 = 2$

Table 2. Results of Fits to ^{2}H and ^{17}O MRD Profiles from Immobilized BPTI[a]

parameter (unit)	value	
	^{2}H	^{17}O
τ_1 (μs)	5.8 ± 0.3	$[5.8]^b$
S_1 (−)	0.85 ± 0.04	$[0.85]^b$
$\bar{\eta}_1$ (−)	0.26 ± 0.04	
$\tau 2$ (ns)	90 ± 3	50 ± 3
S_2 (−)	1.11 ± 0.01	1.06 ± 0.02

[a] For $N_1 = 2$ and $N_2 = 1$. [b] Parameter values within brackets were frozen in the fit.

or $N_1 = 2$ and $N_2 = 1$. Component 1 is nearly in the slow-exchange limit, $Q_k^2 + L_k^2 \gg 1$, where the R_1 contribution is proportional to N_k/τ_k (section 3) so N_1 cannot be determined from the fit. Fits with N_1 frozen to either 1 or 2 are of similar quality, but the $N_1 = 1$ fit yields an unphysically large asymmetry parameter, $\bar{\eta}_1 \approx 0.8$ (section 3). We therefore conclude that $N_1 = 2$, and hence $N_2 = 1$. The fit then yields the residence times $\tau_1 = 5.8$ μs and $\tau_2 = 90$ ns (Table 2). Since W111 is closest to the protein surface (Figure 1) and has fewer H-bonds than W112 and W113, it should have the shortest residence time. We therefore assign component 2 to W111.

Because component 1 is close to the slow-exchange limit, the dispersion frequency is governed by $\bar{\omega}_{Q,k}$ rather than $1/\tau_k$ (section 3). In this limit, information about the residence time is only conveyed by the dispersion amplitude, which is proportional to $1/\tau_1$. The residence time, τ_1, deduced for component 1 should therefore be interpreted as a harmonic average

$$\frac{1}{\tau_1} = \frac{1}{2}\left(\frac{1}{\tau_{W112}} + \frac{1}{\tau_{W113}}\right) \qquad (10)$$

which is dominated by the shorter of the two residence times. It is possible that both water molecules exchange in the same partial unfolding event, in which case $\tau_{W112} = \tau_{W113} = 5.8$ μs (Table 2). But it is also conceivable that one of them (presumably the most deeply buried W113) has a somewhat longer residence time than the other one. In any event, both residence times must be longer than $\tau_1/2 = 2.9$ μs (this follows from eq 10) and neither of them can be much longer than 5.8 μs (since this would bring us back to the rejected $N_1 = 1$ scenario).

The effective order parameter, $S_1 = 0.85$, for W112 and W113 is high, consistent with each of these water molecules being restrained by four H-bonds.[19−22] The motionally induced asymmetry parameter, $\bar{\eta}_1 = 0.26$, is relatively small, as expected for highly ordered water molecules in a highly immobilized protein (section 3).

Since the true order parameter cannot exceed 1, the effective order parameter, $S_{W111} = 1.11$, deduced from the fit indicates that the rigid-lattice quadrupole frequency for W111 is slightly larger than the ice reference value, ω_Q^0 (section 3). This would be the case if one of the deuterons of W111 is not involved in a strong H-bond (or is H-bonded only part of the time).[36] Indeed, all high-resolution crystal structures of BPTI show W111 engaged in two or three H-bonds, whereas each of the other internal water molecules makes four strong H-bonds.[19−22] In the high-pH crystal form,[19,20] W111 donates one H-bond to

(36) Pennanen, T. S.; Lantto, P.; Sillanpää, A. J.; Vaara, J. *J. Phys. Chem. A* **2007**, *111*, 182−192.

Pro8.O and another to Glu7.OE and accepts one H-bond from W112. But the Glu7 side chain is disordered, and in the "open" conformation (30 or 47% population) Glu7.OE is more than 6 Å away from W111, which then donates only one H-bond. In the decameric crystal form at neutral pH,[21,22] Glu7 is entirely in the high-pH "open" conformation (that does not H-bond to W111), but then a sulfate-coordinated water molecule is within H-bonding distance of W111. It is not clear whether this H-bond arrangement would prevail also in the absence of sulfate ions. In any case, W111 is less extensively and less symmetrically H-bonded than the other three internal water molecules, which is consistent with a larger quadrupole frequency.[36]

4.2. BPTI : ^{17}O MRD Profile. We now turn to the ^{17}O MRD profile in Figure 3b. Because the rigid-lattice quadrupole frequency, ω_Q^0, is nearly an order of magnitude larger for ^{17}O than for ^{2}H, the slow-exchange limit is reached for shorter residence times. Therefore, W112 and W113, with residence times of several microseconds, contribute very little to the ^{17}O R_1 dispersion, even though they dominate the ^{2}H dispersion. Indeed, the ^{17}O R_1 profile in Figure 3b is well described by a single EMOR component, apart from the ubiquitous nanosecond component (section 4.7). The expected contribution from W112 and W113 is too small (Figure 3b) to be resolved and it was therefore included with fixed parameter values taken from the ^{2}H fit (Table 2).

The single-fitted EMOR component, which accordingly is assigned to W111, yields a residence time, $\tau_{W111} = 50$ ns, similar to, but significantly shorter than, the value, 90 ns, derived from the ^{2}H data. The ratio of 1.8 of these residence times can be attributed to the different isotopic composition of the solvent in the two cases: H_2O for the ^{17}O data and D_2O for the ^{2}H data (Table 1). The solvent isotope effect is not necessarily the same for all internal water molecules (section 5.2), and it was therefore ignored in the fixed ^{17}O R_1 contribution from W112 and W113. Because this contribution is small, a factor-2 isotope effect would only change the fitted W111 parameters by a few percent. As we found from the ^{2}H data, the effective order parameter, $S_{W111} = 1.06$, is slightly larger than 1. The likely explanation is the same: the incomplete and unsymmetrical H-bond complement of W111 makes the ^{17}O rigid-lattice quadrupole frequency slightly larger than the ice reference value, ω_Q^0.[36]

For ^{17}O, we also measured the transverse relaxation rate, R_2 (open circles in Figure 3b). Because a general SLT result for transverse relaxation by the EMOR mechanism is not available, we did not include the R_2 data in the fit. Instead, we used the parameter values derived from the R_1 fit to "predict" the R_2 dispersion profile by replacing eq 9 with

$$F_{5/2}(L_k,Q_k,0) = \frac{2}{7}\left[\frac{0.3}{1+Q_k^2} + \frac{0.5}{1+Q_k^2+L_k^2} + \frac{0.2}{1+Q_k^2+4L_k^2}\right] + \frac{5}{7}$$
$$\left[\frac{0.3}{1+4Q_k^2} + \frac{0.5}{1+4Q_k^2+L_k^2} + \frac{0.2}{1+4Q_k^2+4L_k^2}\right] \quad (11)$$

This is not a rigorous result, but rather an ad hoc interpolation formula that reduces correctly to the known forms in the low-field ($L_k^2 \ll 1 + Q_k^2$) and BWR ($Q_k^2 \ll 1$) limits. Provided that a frequency-independent offset of 120 s^{-1} is included, this formula reproduces the experimental R_2 dispersion profile rather well (dashed curve in Figure 3b). The origin of the offset may be a deficiency in the ad hoc eq 11 or a secondary relaxation
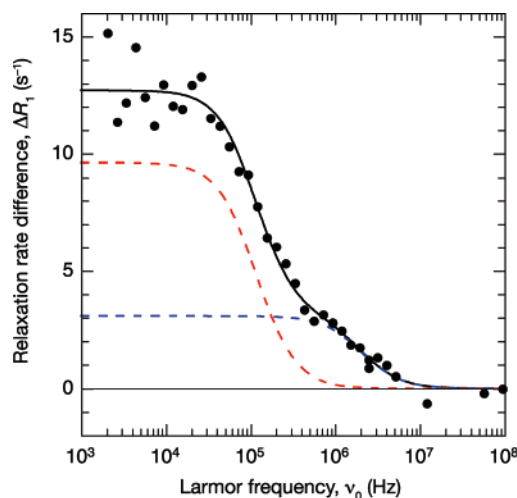
Figure 4. Difference of water ^{2}H MRD profiles from immobilized BPTI at pD 4.4 and 6.5. The data were measured on samples B2 (pD 6.5) and B3 (pD 4.4) and were normalized to $N_W = 3000$ before taking the difference. The solid curve was obtained by fitting the model to the R_1 data as described in the text. The dashed curves are the two COOD components.

mechanism. Scalar relaxation of the second kind, by proton-exchange modulation of the ^{1}H−^{17}O J coupling, can produce such an offset, but the scalar R_2 is less than 1 s^{-1} at pH 4.1 in bulk H_2O[37] and presumably even less in the presence of protein (which also catalyzes proton exchange).

4.3. BPTI : ^{2}H pD Dependence. Whereas ^{17}O relaxation exclusively monitors the dynamics of water molecules, ^{2}H relaxation may also contain a contribution from labile protein deuterons that exchange sufficiently rapidly with water deuterons.[17,38] This labile-D contribution can dominate R_1 at low or high pD,[13] but in the pD range 4.4 − 6.5 of our BPTI samples it is quite small. Nevertheless, after normalizing R_1 to the same protein concentration (same N_W value), we find that the ^{2}H MRD profile recorded at pD 4.4 lies significantly above the one measured at pD 6.5 (Figure 4). At these pD values, ND deuterons exchange too slowly to contribute to R_1.[13,38] Furthermore, the 8 hydroxyl deuterons in BPTI all have acid-catalyzed exchange rate constants less than 10^7 M^{-1} s^{-1} at 20 °C[38,39] so that, even at pD 4.4, the hydroxyl deuteron residence time is greater than 1 ms. As for W122 (with a residence time of 0.4 ms), the R_1 contribution from the hydroxyl deuterons is therefore negligibly small.

The R_1 difference shown in Figure 4 must therefore be produced by labile deuterons in carboxyl groups. The pK_a values of the 5 COOD groups in BPTI have been determined from ^{13}C shift titrations.[40] After applying a small temperature correction,[41] we obtain, for the mean number of COOD deuterons in BPTI, $N_{COOD} = 1.23$ at pD 4.4 and $N_{COOD} = 0.015$ at pD 6.5. The ^{2}H MRD profile at pD 6.5 (Figure 3a) can therefore be attributed exclusively to water deuterons.

We assume that the EMOR contributions from W111−W113 as well as the high-frequency hydration contributions are independent of pH, so that they cancel out in the difference,

(37) Halle, B.; Karlström, G. *J. Chem. Soc., Faraday Trans. 2* **1983**, *79*, 1031−1046.
(38) Denisov, V. P.; Halle, B. *J. Mol. Biol.* **1995**, *245*, 698−709.
(39) Liepinsh, E.; Otting, G.; Wüthrich, K. *J. Biomol. NMR* **1992**, *2*, 447−465.
(40) Richarz, R.; Wüthrich, K. *Biochemistry* **1978**, *17*, 2263−2269.
(41) March, K. L.; Maskalick, D. G.; England, R. D.; Friend, S. H.; Gurd, F. R. N. *Biochemistry* **1982**, *21*, 5241−5251.

$\Delta R_1 \equiv R_1(\text{pD } 4.4) - R_1(\text{pD } 6.5)$. This assumption is consistent with previous solution MRD studies of BPTI over a wide pD range.[38] The difference dispersion, which we thus attribute entirely to COOD deuterons, clearly contains two components (Figure 4). The fit yields two correlation times, $\tau_{\text{COOD,1}} = 0.8 \pm 0.2$ μs and $\tau_{\text{COOD,2}} = 44 \pm 8$ ns, and two amplitude parameters, $N_{\text{COOD,1}}S^2_{\text{COOD,1}} = 0.10 \pm 0.03$ and $N_{\text{COOD,2}}S^2_{\text{COOD,2}} = 0.62 \pm 0.05$. These amplitudes were obtained with a rigid-lattice quadrupole frequency, $\omega^0_Q = 8.2 \times 10^5$ s^{-1}, derived from NQR studies of amino acid crystal hydrates.[42]

The dominant exchange mechanism for the COOD deuteron is thought to involve a cyclic H-bonded configuration with two water molecules linking the carboxylic oxygen atoms. With this mechanistic assumption, NMR relaxation data on acetic acid solutions yield a COOD deuteron residence time of 0.4 ± 0.1 μs in acetic acid/D$_2$O solution at 25 °C.[43] Considering that Glu and Asp COOD groups in proteins are only partially solvent-exposed, we expect somewhat longer COOD residence times in BPTI. The correlation time, 0.8 μs, for component 1 is therefore most likely a COOD residence time.

The shorter correlation, 44 ns, might reflect more efficient deuteron transfer in a COOD/COO$^-$ pair linked by one or two water molecules, as proposed for partially neutralized poly-(acrylic acid).[44] The COOD groups of Glu49 and Asp50 are sufficiently close (~6 Å) for this mechanism to operate. On the basis of the pK_a values of these residues, we would then have $N_{\text{COOD,2}} = 0.55$ and thus $S_{\text{COOD,2}} = 1.06 \pm 0.04$. But an order parameter near 1 is unlikely for the highly exposed Glu49, considering that $S_{\text{COOD}} = 0.35$ for the similarly exposed Asp and Glu side chains in the collagen triple helix.[13]

We therefore favor an alternative interpretation, where component 1 represents the exchange (EMOR mechanism) of all 1.23 COOD deuterons and component 2 reflects slow internal motions of one or more of the Glu and Asp side-chains. (At pD 4.4, the two Glu residues account for 67% of N_{COOD}.) The amplitude of component 1 then yields $S_{\text{COOD}} = 0.29 \pm 0.04$, more in line with the collagen result.[13] Side-chain conformational dynamics occurs on several time scales and we can associate separate order parameters with fast (picosecond) librations ($S^{\text{fast}}_{\text{COOD}}$) and with slower (nanosecond) larger-scale conformational transitions ($S^{\text{slow}}_{\text{COOD}}$). An indication that Glu7 does, in fact, undergo a slow conformational transition is provided by crystal structures implying that the COOD group of Glu7 moves by ~5 Å between two conformations with comparable populations.[19,20] The order parameter, $S_{\text{COOD}} = 0.29$, that appears in the amplitude of component 1 is the product $S^{\text{fast}}_{\text{COOD}}S^{\text{slow}}_{\text{COOD}}$, and the amplitude of component 2 is $N_{\text{COOD}}(S^{\text{fast}}_{\text{COOD}})^2[1 - (S^{\text{slow}}_{\text{COOD}})^2]$. With $N_{\text{COOD}} = 1.23$, as for component 1, this yields $S^{\text{fast}}_{\text{COOD}} = 0.77$ and $S^{\text{slow}}_{\text{COOD}} = 0.38$. We note that this analysis is based on the assumption that the protein is highly immobilized in the gel network (section 4.7).

4.4. BPTI : ^{2}H Temperature Dependence. The EMOR mechanism, which attributes the relaxation dispersion to exchange of internal water molecules, makes definite predictions about the temperature dependence of R_1. This dependence is particularly simple at low frequencies, where the intrinsic
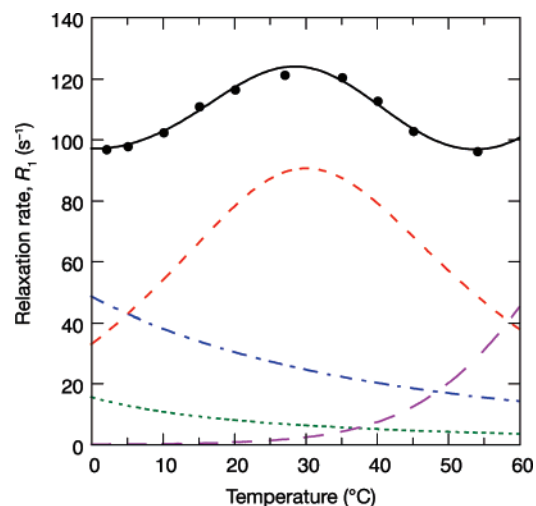
(42) Edmonds, D. T. *Phys. Rep.* **1977**, *29*, 233−290.
(43) Lankhorst, D.; Schriever, J.; Leyte, J. C. *Chem. Phys.* **1983**, *77*, 319−340.
(44) Lankhorst, D.; Schriever, J.; Leyte, J. C. *Macromolecules* **1984**, *17*, 93−100.

Figure 5. Temperature dependence of water ^{2}H relaxation rate, R_1, at 1.5 kHz for immobilized BPTI at pD 4.4 (sample B3, $N_W = 3615$). The solid curve was obtained by fitting the model to the R_1 data as described in the text. The broken curves are the contributions to R_1 from internal water molecules W111 (blue), W112 and W113 (red), and W122 (magenta) and from bulk and surface hydration water (green).

relaxation rate, $R_{1,k}$, has reached its zero-frequency limit, $R_{1,k}$-(0). At low temperatures, where the internal water molecule k is in the slow-exchange limit ($\bar{\omega}_{Q,k}\tau_k \gg 1$), $R_{1,k}(0)$ is inversely proportional to the residence, τ_k, and therefore increases with temperature as τ_k becomes shorter. At high temperatures, in the fast-exchange or BWR regime ($\bar{\omega}_{Q,k}\tau_k \ll 1$), $R_{1,k}(0)$ is proportional to τ_k and therefore decreases with temperature. Each EMOR component k should thus give rise to a maximum in $R_1(0)$ at the temperature where $\tau_k \approx 1/\bar{\omega}_{Q,k}$, which is on the order 10^{-6} s for ^{2}H. This behavior is illustrated, for the special case $\bar{\eta}_k = 0$, by eq 8 and Figure 2.

At low frequencies, the ^{2}H relaxation rate is dominated by component 1, assigned to internal water molecules W112 and W113 (Figure 3a). Since the residence time, $\tau_1 = 5.8$ μs, at 20 °C is longer than $1/\bar{\omega}_{Q,k}$, we expect a maximum in R_1 at slightly higher temperature. To test this prediction, we measured the water ^{2}H relaxation rate, R_1, at the lowest accessible frequency, 1.5 kHz, for immobilized BPTI (sample B3) as a function of temperature. A maximum is, indeed, observed at ~30 °C (Figure 5).

For the quantitative analysis of the temperature dependence in Figure 5, we model R_1 as a sum of four components. Three of these are the same as in Figure 3a, with the only difference that the small COOD contribution (9% of R_1 at 20 °C) present at pD 4.4 is lumped together with W111 as component 2. The fourth component is W122, which only contributes at higher temperatures. At 1.5 kHz, all EMOR components can be taken to be in the zero-frequency ("extreme narrowing") limit, since $L^2_k \ll 1$ for $\tau_k < 30$ μs and for longer residence times the contribution to R_1 is negligibly small.

The small contribution from bulk and surface hydration water was forced to agree with the fit in Figure 3a at 20 °C and was taken to have the same relative temperature variation as $R_{1,\text{bulk}}$.[45] EMOR component 1 (W112 and W113) and 3 (W122) were described with the exact SLT expression (section 3) with fixed $\bar{\eta}_k = 0.26$ (Table 2). The temperature dependence of the

(45) Hindman, J. C. *J. Chem. Phys.* **1974**, *60*, 4488−4496.

residence times was modeled with two parameters in an Arrhenius expression

$$\tau_k(T) = \tau_k(T_0) \exp\left[\frac{E_k^{\ddagger}}{R}\left(\frac{1}{T} - \frac{1}{T_0}\right)\right] \qquad (12)$$

with the reference temperature $T_0 = 293$ K. For W122, we adopt $\tau_3(T_0) = 0.4$ ms and the activation energy, $E_3^{\ddagger} = 90$ kJ mol^{-1}, from a previous solution MRD study.[14] The order parameter, $S_3 = 0.95$, is taken from the same source.[14] Component 2 (W111 and COOD) is in the BWR regime at all investigated temperatures, so it can be modeled as

$$f_2 R_{1,2}(T) = f_2 R_{1,2}(T_0) \exp\left[\frac{E_2^{\ddagger}}{R}\left(\frac{1}{T} - \frac{1}{T_0}\right)\right] \qquad (13)$$

where $f_2 R_{1,2}(T_0)$ is forced to agree with the fit in Figure 3a at 20 °C.

The fit in Figure 5 gave the following parameter values: $E_2^{\ddagger} = 16 \pm 2$ kJ mol^{-1}, $E_1^{\ddagger} = 43 \pm 1$ kJ mol^{-1}, $\tau_1(T_0) = 3.9 \pm 0.1$ μs and $S_1 = 0.45 \pm 0.01$. Bearing in mind the several simplifying assumptions in this analysis, the close agreement for the residence time, τ_1 (for W112 and W113), deduced from the full dispersion profile at 20 °C (5.8 μs) and from the temperature dependence at 1.5 kHz (3.9 μs) is reassuring. The activation energy, 43 kJ mol^{-1}, is also in the expected range, intermediate between the faster exchanging W111 and the more long-lived W122. The order parameter, S_1, deduced from the temperature dependence (0.45) is significantly lower than the one obtained from the full dispersion profile (0.85), but $R_1(0)$ depends only weakly on S_1 near the maximum so this parameter is likely to absorb any short-comings of the simplified model.

Another notable result, apart from consistent τ_1 values, is the small amplitude of the R_1 maximum. The measured $R_1(0)$ values vary by only 25%, as compared to more than a factor 2 in a similar experiment on an agarose gel.[12] The temperature dependence in R_1 is weaker for BPTI because the different EMOR components have opposite temperature dependencies (Figure 5). On the low-temperature flank of the maximum, the increase of $R_{1,1}(0)$ is counteracted by the decrease of $R_{1,2}(0)$ and the bulk and surface hydration contribution. On the high-temperature flank, the decrease of $R_{1,1}(0)$ is counteracted by the sharp increase of $R_{1,3}(0)$ owing to the high activation energy of W122. The contribution from W122 is predicted to produce another maximum in $R_1(0)$ near 75 °C. Although BPTI should remain folded at this temperature, our measurements at these high temperatures were not included in the analysis because of doubts about the integrity of the gel network. At the reported temperatures, no significant irreversible changes were detected.

4.5. Ubiquitin: ²H MRD Profile. Whereas BPTI contains four internal water molecules, ubiquitin has only one (Figure 1). This water molecule, labeled W28, is superficially buried and makes only two H-bonds with protein backbone atoms.[26-28] A third H-bond involves an external water molecule[27,28] or, possibly, the side-chain of Lys27.[26,27] With regard to burial depth and H-bonding, W28 in ubiquitin is similar to W111 in BPTI. We therefore expect the residence time of W28 to be of the same order of magnitude as for W111.

Figure 6 shows water ²H and ¹⁷O MRD profiles from immobilized ubiquitin. As for BPTI, the profiles show a high-frequency dispersion with a correlation time of a few nanosec-
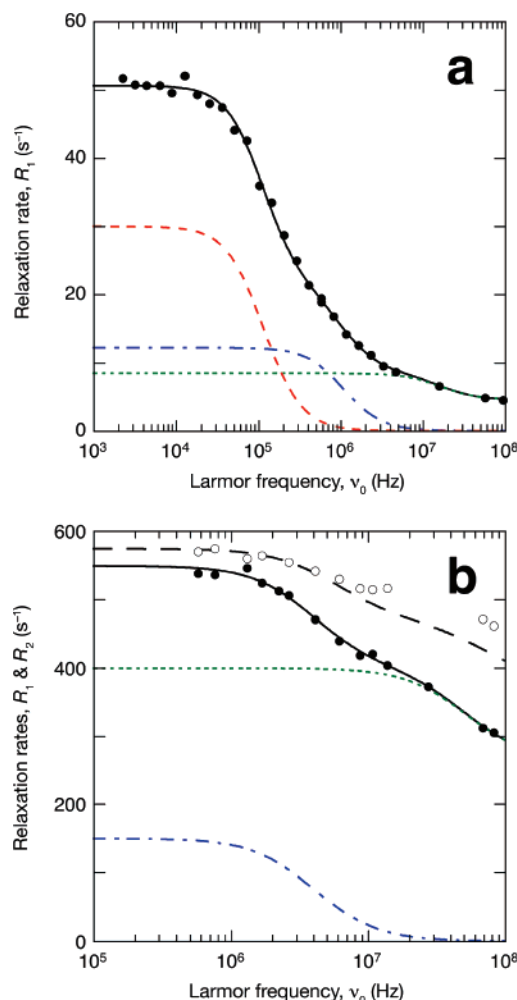

Figure 6. Water ²H (a) and ¹⁷O (b) MRD profiles from immobilized ubiquitin at 20 °C. The data were measured on samples U2 (a) and U1 (b) and are normalized to $N_W = 3000$. Filled and open circles represent R_1 and R_2 data, respectively. The solid curves were obtained by fitting the model to the R_1 data as described in the text. The broken curves are the contributions to R_1 from the internal water molecule W28 (blue), from COOD deuterons (red), and from bulk and surface hydration water (green). The parameter values resulting from the fits are given in Table 3. In panel (b), the dashed R_2 profile was computed from the parameters obtained from the R_1 fit.

onds, which we attribute to external hydration (section 4.7). In addition, one (¹⁷O) or two (²H) low-frequency EMOR components are evident. Whereas the number of resolved EMOR components in the MRD profile is the same as for BPTI, their amplitudes are much smaller for ubiquitin (cf. Figures 3 and 6, where all MRD profiles refer to the same water/protein mole ratio, $N_W = 3000$). This difference is in the expected direction, but a detailed analysis is required to ascertain whether the MRD data are quantitatively consistent with the known differences in structural hydration between BPTI and ubiquitin.

The fit to the ²H MRD profile in Figure 6a requires two EMOR components. The correlation times are sufficiently short that the BWR limit is applicable. The fit therefore yields the amplitude parameter $N_k S_k^2$, rather than N_k and S_k separately, and it is independent of $\bar{\eta}_k$. The residence times for the two components are $\tau_1 = 0.78$ μs and $\tau_2 = 83$ ns (Table 3). The dominant component 1 must be assigned to COOD deuterons, because it is not present in the ¹⁷O profile (see below). Moreover, the residence time, 0.8 μs, for component 1 coincides

Table 3. Results of Fits to ^{2}H and ^{17}O MRD Profiles from Immobilized Ubiquitin

	value	
parameter (unit)	^{2}H	^{17}O
$\tau 1$ (ms)	0.78 ± 0.03	
$N_1 S_1^2$ (−)	0.34 ± 0.02	
$\tau 2$ (ns)	83 ± 5	23 ± 3
$N_2 S_2^2$ (−)	0.58 ± 0.03	0.35 ± 0.07

with the COOD residence time in BPTI (section 4.3). Ubiquitin contains 12 COOD groups, including several Glu residues with upshifted pK_a values. From the known pK_a values and Hill coefficients,[46] we find (after a small temperature correction[41]) $N_{COOD} = 1.99$ at pD 5.3 (sample U2). We thus expect a larger COOD contribution than for BPTI (with $N_{COOD} = 1.23$) and this is, indeed, the case (cf. Figures 4 and 6a). With $N_1 = 1.99$, the amplitude parameter $N_1 S_1^2$ yields $S_{COOD} = 0.42 \pm 0.01$, slightly higher than for collagen[13] (0.35) or BPTI (0.29).

Component 2 is assigned to the single internal water molecule (W28) in ubiquitin. With $N_2 = 1$, the amplitude parameter $N_2 S_2^2$ yields $S_{W28} = 0.76 \pm 0.02$. As for W111 in BPTI (section 4.1), the incomplete H-bonding of W28 is likely to increase its quadrupole frequency above the ice reference value, so the true order parameter of W28 is probably slightly lower than 0.76. Furthermore, component 2 might contain an unresolved contribution from slow internal motions of Glu and Asp side chains (as for BPTI, see section 4.3). This would increase the apparent order parameter, S_2, and could shift the apparent residence time in either direction, depending on whether the internal motion correlation time is shorter or longer than the residence time of W28.

4.6. Ubiquitin: ^{17}O MRD Profile. As expected, the ^{17}O MRD profile reveals only one EMOR component, which we assign to internal water W28. (For consistency with the ^{2}H profile, this component is labeled $k = 2$.) The residence time obtained from the fit is 23 ns, a factor 3.6 shorter than the corresponding ^{2}H residence time (Table 3). With $N_2 = 1$, the amplitude parameter $N_2 S_2^2$ yields $S_{W28} = 0.59 \pm 0.06$, significantly smaller than the ^{2}H-derived value (0.76). The factor 3.6 ^{2}H/^{17}O residence time ratio is larger than the expected solvent isotope effect (section 5.2). This discrepancy, as well as the larger ^{2}H order parameter, suggests that component 2 in the ^{2}H MRD profile is the unresolved sum of the W28 contribution and a contribution from internal motions in Glu/Asp side chains on the 50−100 ns time scale.

As for BPTI (Figure 3b), the transverse (R_2) MRD profile was predicted with the aid of eq 11, and the parameter values derived from the fit to the R_1 data. By adding a frequency-independent offset of 20 s^{-1}, we obtain reasonable agreement with the experimental R_2 data (dashed curve in Figure 6b). Although smaller than for BPTI, the offset is an order of magnitude larger than the scalar relaxation rate in bulk H$_2$O at pH 4.9.[37]

4.7. Surface Hydration. The MRD profiles presented here are dominated by dispersion components below $\sim$10 MHz, produced by exchange of long-lived ($>$10 ns) internal water molecules. But the excess relaxation rate, $R_{1,ex}(\omega_0) \equiv R_1(\omega_0) - R_{1,bulk}$, also contains a contribution from the retarded rotational

motion of water molecules interacting with the external surface of the protein. In solution MRD, this surface hydration contribution is operationally defined as that part of $R_{1,ex}$ which is frequency-independent below $\sim$100 MHz (the highest accessible ^{2}H or ^{17}O Larmor frequency).[17,32] The water molecules responsible for this contribution must have correlation times shorter than $\sim$1 ns. At room temperature, about half of the surface hydration contribution comes from relatively few hydration water molecules located in surface pockets and with residence times of several hundred ps.[32,47]

The surface hydration contribution observed for immobilized proteins differs in two ways from that observed for the same proteins in solution. First, the excess relaxation rate, $R_{1,ex}(\omega_0)$, at $\sim$100 MHz is about twice as large as in solution. Second, there is a universal dispersion component with a correlation time of a few nanoseconds, which we also attribute to surface hydration (see below). Both of these contributions are represented by the second term in eq 1. The simplest description of the surface hydration contribution consistent with these observations is of the form

$$f_S[R_{1,S}(\omega_0) - R_{1,bulk}] = f_S^{fast}[R_{1,S}^{fast} - R_{1,bulk}] + f_S^{slow}R_{1,S}^{slow}(0)$$
$$\left[\frac{0.2}{1 + (\omega_0\tau_S^{slow})^2} + \frac{0.8}{1 + (2\omega_0\tau_S^{slow})^2} \right] \quad (14)$$

where $f_S = f_S^{fast} + f_S^{slow}$ and $R_{1,S}^{slow}(0) \gg R_{1,bulk}$. The three independent surface hydration parameters are chosen as the correlation time, τ_S^{slow}, and the two amplitude parameters

$$\frac{N_W}{R_{1,bulk}}f_S^{fast}[R_{1,S}^{fast} - R_{1,bulk}] = N_S^{fast}\left(\frac{\tau_S^{fast}}{\tau_{bulk}} - 1\right) \quad (15)$$

$$\frac{N_W}{\tau_S^{slow}(\omega_Q^0)^2}f_S^{slow}R_{1,S}^{slow}(0) = N_S^{slow}(S_S^{slow})^2 \quad (16)$$

Since our focus was on the low-frequency EMOR components, we did not sample R_1 densely at frequencies above 10 MHz. The values of the surface hydration parameters derived from the fits are therefore sensitive to small measurement errors. Nevertheless, a consistent picture emerges, where both proteins and both nuclides yield similar parameter values: $N_S^{fast}(\tau_S^{fast}/\tau_{bulk} - 1) = (1.9 - 2.6) \times 10^3$, $N_S^{slow}(S_S^{slow})^2 = 2-3$ and $\tau_S^{slow} = 2-7$ ns.

The values for $N_S^{fast}(\tau_S^{fast}/\tau_{bulk} - 1)$ obtained here are larger than the value, $(1.2 \pm 0.1) \times 10^3$, derived from solution MRD studies of BPTI and ubiquitin.[23,38] To see if this difference can be accounted for by the hydration of the glutaraldehyde (GA) crosslinking reagent, we measured the ^{17}O relaxation rate in a H$_2$O solution of GA without protein, obtaining $N_S^{GA}(\tau_S^{GA}/\tau_{bulk} - 1) = 15.6 \pm 0.1$ at 20 °C. Here, N_S^{GA} is the number of water molecules interacting with one GA molecule. By multiplying $N_S^{GA}(\tau_S^{GA}/\tau_{bulk} - 1)$ with the GA/protein mole ratio, N_{GA}, from Table 1, we find that GA hydration can account for at most half of the increase of $N_S^{fast}(\tau_S^{fast}/\tau_{bulk} - 1)$ in the protein gels. Moreover, the frequency-dependent part of the surface hydration contribution, modeled by the second term of eq 14, is not present in solution. If it existed in solution, this dispersive component would not have escaped detection, since it would be comparable

(46) Sundd, M.; Iverson, N.; Ibarra-Molero, B.; Sanchez-Ruiz, J. M.; Robertson, A. D. *Biochemistry* **2002**, *41*, 7586−7596.

(47) Modig, K.; Liepinsh, E.; Otting, G.; Halle, B. *J. Am. Chem. Soc.* **2004**, *126*, 102−114.
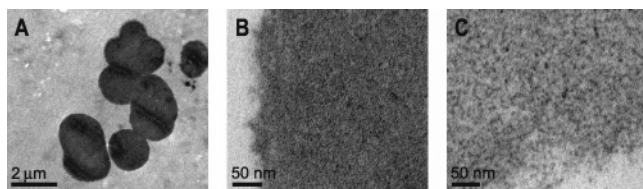
Figure 7. Transmission electron micrographs of ubiquitin gel sample U2 (A and B) and BPTI gel sample B3 (C).

in amplitude and frequency to the internal water contribution. Consequently, the additional fast surface hydration contribution and the nanosecond surface hydration contribution must both be, direct or indirect, effects of protein crosslinking.

The protein concentrations used here (Table 1), 7−11% by volume, are comparable to or lower than the BPTI and ubiquitin concentrations used in previous solution MRD studies of these proteins.[14,23,24,35,38,47,48] The water/protein mole ratio, N_W, is an order of magnitude higher than the number, $N_S = N_S^{fast} + N_S^{slow}$, of water molecules in the first hydration layer of the protein. On average, the protein molecules are separated by ∼10 water diameters, a distance that could easily be spanned by cross-links of ∼8 GA molecules (as implied by the 4:1 GA:Lys stoichiometry of the crosslinking reaction[30]). So if the protein molecules were uniformly distributed in space, we should see essentially the same surface hydration contribution to R_1 as in solution. Because this is not the case, we conclude that the spatial distribution of protein molecules in the gel is inhomogeneous.

BPTI is known to self-assemble into a compact decamer at high salt concentrations.[48,49] Based on ^{1}H MRD studies of ∼7 vol % BPTI solutions, it was estimated that ∼5% of the protein is present in decamer form in the absence of added salt.[48] The decamer fraction in our samples should be even lower, because of cross-link interference. While decamer formation may affect the slow conformational fluctuations that govern the rate of internal water exchange, the burial of protein surface in the decamer should decrease, rather than increase, the surface hydration contribution.

Although a uniform distribution of crosslinked protein molecules is geometrically feasible, the actual gel structure may be formed under kinetic control. Once two protein molecules have been connected by a cross-link, the next cross-link is more likely to bridge the already connected pair than to involve a new protein molecule. The gel might thus consist largely of dense clusters of highly crosslinked protein molecules, connected by less extensively crosslinked protein molecules. Morphological characterization by transmission electron microscopy (the sample preparation protocol is decribed in Supporting Information) showed that the (translucent) BPTI gel is homogeneous on length scales above a few hundred Å, whereas the (opaque) ubiquitin gel contains μm-sized domains of higher protein density (Figure 7). However, heterogeneity on shorter length scales cannot be excluded at this resolution. The gel structure is not regular so there must exist a distribution of protein−protein separations. If this distribution is sufficiently wide that the hydration layers of some protein molecules make contact or even overlap, then the observed average dynamic perturba-

(48) Gottschalk, M.; Venu, K.; Halle, B. *Biophys. J.* **2003**, *84*, 3941−3958.
(49) Hamiaux, C.; Pérez, T.; Prangé, S.; Vessler, M.; Riès-Kautt, M.; Vachette, P. *J. Mol. Biol.* **2000**, *297*, 697−712.

tion, as measured by the parameter $N_S^{fast}(\tau_S^{fast}/\tau_{bulk} - 1)$, will be larger than in a protein solution, where the protein molecules tend to stay as far apart as possible. Some protein molecules in the gel may be sufficiently close to produce hydration sites with nanosecond residence times, thus accounting for the dispersive surface hydration component. The actual situation is likely to be more complex than can be captured by our parsimonious 3-parameter description. In particular, the external hydration water in the gel may exhibit a wide range of correlation times, from a few picoseconds to a few nanoseconds. Hydration dynamics in protein gels is of interest per se, for example, as a model for more complex biological systems, but our objective here is to characterize protein and internal water dynamics. The nanosecond hydration dynamics then simply defines a lower limit of ∼10 ns for the time scales of internal dynamics that can be studied by the present method.

4.8. Validation of the EMOR/MRD Method. Proteins can be immobilized by direct protein−protein interactions, as in physical gels or crystals. Chemical crosslinking is an attractive alternative, because the protein remains fully hydrated. Ideally, crosslinking quenches the global translational and rotational motions without affecting the internal protein dynamics. To validate the EMOR/MRD method for studying internal protein dynamics, we must show that this ideal is at least approached in crosslinked gels. We have done this by varying the composition of the gel and by comparing with solution MRD results.

As discussed in Supporting Information, the results in Figure S1 demonstrate that the protein dynamics that govern internal water exchange are essentially unaffected by substantial variations in protein and crosslinker concentrations. At low frequencies, R_1 is dominated by EMOR component 1 (W112 and W113), which is roughly inversely proportional to τ_1. Since the residence times determined here span several orders of magnitude, a few percent variation is clearly inconsequential. We note also that the shoulder in the MRD profile just below 1 MHz, attributed to EMOR component 2 (W111), occurs at the same frequency in all profiles.

Using parameter values derived from MRD profiles of immobilized proteins and an independent estimate of the protein rotational correlation time, τ_{RP}, we can predict the solution MRD profile. By comparing predicted and measured solution MRD profiles, we can then check the mutual consistency of the two methods. Solution MRD does not usually yield residence times directly (only lower and upper bounds), so we focus on the amplitude parameter. The effective amplitude parameter obtained from a solution MRD profile is[17]

$$[N_k S_k^2]_{eff} = \frac{N_k S_k^2}{[1 + (\omega_Q^0 S_k)^2 \tau_{RP} \tau_k]^{1/2}} \quad (17)$$

In the fast-exchange limit, which for an internal water molecule in a freely tumbling protein is defined as $R_{1,k}(0)\tau_k \ll 1$, the denominator in eq 17 is unity and the MRD profile yields the true amplitude parameter, $N_k S_k^2$.

With parameter values from Tables 2 and 3 inserted into eq 17, we can calculate the total effective amplitude parameter, $[NS^2]_{eff} \equiv \sum_k [N_k S_k^2]_{eff}$, that would be obtained from MRD profiles of D_2O solutions of BPTI and ubiquitin at 20 °C. Since the early MRD studies of BPTI and ubiquitin used D_2O solutions also for [17]O measurements,[14,23,24] we use residence times

Table 4. Predicted and Measured Solution MRD Amplitude Parameters

protein	water, k	$[N_k S_k^2]_{eff}$		data source
		^{2}H	^{17}O	
BPTI, immobilized	W111	1.23 ± 0.03	1.11 ± 0.04	Table 2
BPTI, immobilized	W112−113	1.43 ± 0.13	0.98 ± 0.09	Table 2
BPTI, immobilized	W111−113	2.66 ± 0.13	2.09 ± 0.10	Table 2
BPTI, solution	W111−113	2.7 ± 0.1	2.1 ± 0.2	ref 24[a]
ubiquitin, immobilized	W28		0.35 ± 0.07	Table 3
ubiquitin, solution	W28		0.3 ± 0.1	ref 23[b]

[a] BPTI-G36S in D_2O, N_W = 1890, pD 5.6, 27 °C, bi-Lorentzian fit.
[b] Ubiquitin in D_2O, N_W = 3523, pD 5.8, 27 °C, bi-Lorentzian fit.

pertaining to this solvent. For BPTI, we consider the Gly36Ser mutant, lacking the most long-lived internal water molecule, W122.[14,24] We find that the fast-exchange limit is valid to within 1% or better in all cases considered, except for the BPTI W112−113 component of the ^{17}O dispersion profile, where the denominator in eq 17 equals 1.48 (for τ_{RP} = 5 ns). The effective correlation time for this component should be reduced by the same factor as the amplitude,[17] which explains why the effective ^{2}H correlation time was found to be 20% longer than the effective ^{17}O correlation time. At the high BPTI concentration (N_W = 1890) used in the solution MRD study,[14,24] a significant fraction of the protein may have formed decamers,[48] consistent with the observed deviation from single-Lorentzian dispersion shape.[14,24] We therefore redetermined the amplitude parameter from a bi-Lorentzian fit.

As seen from Table 4, the effective amplitude parameter predicted from the present data on immobilized proteins agrees quantitatively with the corresponding parameter derived from the solution MRD profile. This agreement, for both BPTI and ubiquitin, strongly supports our proposal that water ^{2}H and ^{17}O relaxation from immobilized proteins is governed by the EMOR mechanism.

A further important implication of this agreement is that the orientational order parameter, S_k, of internal water molecules is essentially the same in immobilized and freely tumbling proteins. This need not be the case, because S_k reflects orientational averaging on very different time scales in the two cases. For freely tumbling proteins, S_k can only be affected by internal motions faster than the protein tumbling time, τ_{RP}, or ∼5 ns for the proteins considered here. For immobilized proteins, S_k is averaged by all internal motions experienced by the water molecule during its residence time, τ_k, or ∼6 μs for W112 and W113 in BPTI. We can thus conclude that internal motions slower than a few nanoseconds do not contribute significantly to orientational averaging of internal water molecules. It seems likely that most of this averaging is effected by water librational modes on the picosecond time scale.[35]

5. Concluding Discussion

5.1. Spin Relaxation Mechanism. A typical internal water molecule is highly restrained by H-bonds to protein atoms, but once it escapes into the external solvent its orientation is randomized within picoseconds. We have developed a theory of nuclear spin relaxation by this mechanism of exchange-modulated orientational randomization (EMOR),[11] and we have shown here that it accounts quantitatively for the ^{2}H and ^{17}O MRD profiles from immobilized BPTI and ubiquitin. (i) The number of internal water molecules deduced from the MRD data agrees with the crystal structures and the residence times and order parameters of these water molecules are quantitatively consistent with the (less detailed) results obtained from previous solution MRD studies. (ii) The non-monotonic temperature dependence of R_1 is consistent with the values of the residence times and with their expected strong temperature dependence. (iii) The pD dependence of the ^{2}H MRD profile is consistent with the known number of labile deuterons and their exchange rate constants.

Several groups have reported ^{1}H or ^{2}H MRD profiles from crosslinked or otherwise immobilized proteins, but the data have been interpreted with models based on ad hoc assumptions that are inconsistent with the current understanding of hydrated proteins. Thus, the ^{2}H relaxation dispersion from immobilized bovine serum albumin (the only immobilized protein studied by ^{2}H MRD up to now) was attributed to slow motions of hydration water at the protein surface.[50−53] If this hypothesis were correct, MRD data would provide little or no information about protein conformational dynamics. More specifically, Kimmich *et al.* assumed that spin relaxation is induced by water reorientation mediated by slow translational diffusion of water molecules over the rugged protein surface.[50] However, this mechanism can account for the observed MRD profile only if most of the several hundred water molecules at the protein surface have residence times exceeding 1 μs, 5 orders of magnitude above the value established by subsequent MRD and simulation studies.[32]

Koenig et al. postulated that proteins have a small number (two in the case of serum albumin) of special hydration sites with 1 μs residence time on their surfaces.[51−53] According to the EMOR mechanism, the MRD profile would then be dominated by water exchange from these sites. Koenig proposed that water molecules that can make four H-bonds to protein surface atoms have a residence time of 1 μs. However, subsequent MRD studies[17,18,54] and molecular dynamics simulations of many proteins have shown that only buried water molecules have residence times longer than ∼10 ns (at room temperature). Long water residence times are not produced by water−protein H-bonds *per se*, which are not stronger than the short-lived water−water H-bonds. Instead, the long residence times result from entrapment of water molecules in small cavities within the protein structure, which is maintained by intramolecular residue−residue interactions as well as by (global) protein−water interactions. Indeed, it is because the residence times of buried water molecules are determined by structural fluctuations that the MRD profile can provide information about protein dynamics.

The present work departs from these earlier MRD studies also with regard to the underlying spin relaxation theory. The conventional perturbation theory of nuclear spin relaxation is not valid for correlation times on an order of 1 μs and longer (in the case of ^{2}H relaxation).[31] To analyze MRD profiles from immobilized proteins, which are usually dominated by microsecond motions, it is therefore necessary to use a more general

(50) Kimmich, R.; Gneiting, T.; Kotitschke, K.; Schnur, G. *Biophys. J.* **1990**, *58*, 1183−1197.
(51) Koenig, S. H.; Brown, R. D.; Ugolini, R. *Magn. Reson. Med.* **1993**, *29*, 77−83.
(52) Koenig, S. H.; Brown, R. D. *Magn. Reson. Med.* **1993**, *30*, 685−695.
(53) Koenig, S. H. *Biophys. J.* **1995**, *69*, 593−603.
(54) Denisov, V. P.; Halle, B. *Faraday Discuss.* **1996**, *103*, 227−244.

relaxation theory. Our data analysis is based on a rigorous theory of spin relaxation by the EMOR mechanism, valid for arbitrarily long residence times.[11] If MRD data from immobilized proteins are analyzed with the EMOR model but within the framework of the conventional relaxation theory,[51–53] the number of long-lived water molecules will be severely underestimated.[55] Even more importantly, the failure to recognize that the conventional relaxation theory breaks down for long correlation times led previous workers to postulate the existence of universal hydration sites with a temperature-independent residence time of 1 μs.[51–53] In fact, this apparent correlation time is the inverse of the deuteron quadrupole frequency, which acts as an intrinsic low-frequency cutoff on the molecular motions that can induce spin relaxation.[55]

The great majority of previous MRD studies of immobilized proteins have utilized the ^{1}H nuclide. The interpretation of ^{1}H MRD data from immobilized macromolecules is complicated by effects of cross-relaxation and spin diffusion.[56,57] Koenig et al. have analyzed ^{1}H MRD profiles from immobilized proteins in much the same way as ^{2}H profiles, that is, by postulating long-lived surface hydration sites and by using conventional relaxation theory.[51–53] More recently, Korb and Bryant have used a radically different approach to analyze ^{1}H MRD data from crosslinked lysozyme.[58–60] They argue that the molecular motions responsible for the water-^{1}H MRD profile are small-amplitude collective vibration modes in the protein on the 10^{-8}–10^{-5} s time scale. The relaxation mechanism invoked by these authors is known to operate in solids,[31] but it fails by orders of magnitude to account for the ^{1}H MRD profile from immobilized proteins unless one postulates that the vibration modes propagate in a space of reduced dimensionality. Similar models, featuring overdamped vibrations in a polymer chain[61,62] or one-dimensional diffusion of structural defects,[63,64] had been proposed earlier to interpret water ^{1}H relaxation data from biological materials. To account for the observed ^{1}H MRD profile, Korb and Bryant assume that the vibrational density of states for the protein scales as $\omega^{1/3}$ from 10^4 to 10^8 Hz. However, both vibrational spectroscopy[65,66] and computer simulations[67,68] indicate a classical ω^2 scaling up to $\sim 10^{12}$ Hz, as expected for a three-dimensional solid. Apart from its questionable physical basis, this model cannot explain the dependence of the present data on temperature or pD and it cannot rationalize the large difference between the MRD profiles from BPTI and ubiquitin.

We have previously reported ^{2}H MRD data from physical gels of agarose[12] and gelatin.[13] Those extensive data sets could be quantitatively rationalized in terms of the EMOR model. Moreover, we have shown that the ^{1}H MRD data from the same gels[57] are also explained by the EMOR model, modified to include cross-relaxation effects.[56] These studies provided new information about structure, dynamics, and hydration in these structurally complex gels. However, the BPTI and ubiquitin gels examined here allow us to test the EMOR model in a more decisive way, since the structure and internal hydration of these proteins are known. We have also measured the ^{1}H MRD profiles from crosslinked BPTI and ubiquitin. These results, which will be reported elsewhere, underscore the central importance of the EMOR mechanism for understanding the molecular basis of water ^{1}H relaxation in biological tissues and of endogenous image contrast in clinical magnetic resonance imaging.

5.2. Protein Dynamics. In this first application of the MRD/EMOR method to proteins, we have determined the residence times of four internal water molecules. These buried water molecules are an integral part of the protein structure and their exchange is inextricably linked to the structural dynamics of the protein. Our results thus provide direct evidence for large-scale conformational fluctuations on time scales from 20 ns to 6 μs. As expected, the residence times correlate with burial depth. The most superficially buried water molecules, W111 in BPTI and W28 in ubiquitin, have residence times of 80–90 ns (in D_2O at 20 °C). The exchange mechanism for these water molecules likely involves dihedral transitions in one or two obstructing side chains, to allow an external water molecule to replace the internal one in a more or less concerted manner, where each water molecule retains at least two H-bonds at all times. In the case of W111 in BPTI, the crystallographically disordered side chain of Glu7 is most probably involved in the exchange mechanism (Figure 1 and section 4.1). The most long-lived water molecule, W122, in BPTI (0.4 ms at 20 °C, as determined by solution MRD[14]) is buried in a densely packed region near the 14–38 disulfide bridge. The remaining two water molecules, W112 and W113, are intermediate between W111 and W122 in burial depth as well as in residence time (6 μs). The exchange mechanism for W112 and W113 is likely to involve rotation of the Lys41 side chain, exposing these two water molecules to external solvent (Figure 1c), and a slight separation of the backbones of the two flanking loops, allowing external water molecules in the groove to replace W112 and W113 in a concerted manner. The MRD data imply that both W112 and W113 have residence times of a few μs so they probably exchange together. An alternative exchange mechanism can be envisaged, where the three water molecules W111–W113 exchange by stepwise jumps of the three-water chain in and out of the intact pore (Figure 1a). However, W113 would then have a considerably longer residence time than W112, which is not consistent with our MRD data.

A detailed account of the exchange mechanisms for these and other internal water molecules may be provided by molecular dynamics simulations in the not too distant future. A 200 ns simulation of ubiquitin was recently reported that might have revealed the exchange mechanism of W28, but hydration was not analyzed in that study.[69] As microsecond protein simulations become commonplace, experimentally determined residence times of internal water molecules will serve as benchmarks for assessing the quality of the force field.

(55) Halle, B.; Denisov, V. P. *Biophys. J.* **1995**, *69*, 242–249.
(56) Halle, B. *Magn. Reson. Med.* **2006**, *56*, 60–72.
(57) Vaca Chávez, F.; Halle, B. *Magn. Reson. Med.* **2006**, *56*, 73–81.
(58) Korb, J.-P.; Bryant, R. G. *J. Chem. Phys.* **2001**, *115*, 10964–10974.
(59) Korb, J.-P.; Bryant, R. G. *Magn. Reson. Med.* **2002**, *48*, 21–26.
(60) Korb, J.-P.; Bryant, R. G. *Biophys. J.* **2005**, *89*, 2685–2692.
(61) Rorschach H. E.; Hazlewood, C. F. *J. Magn. Reson.* **1986**, *70*, 79–88.
(62) Hackmann, A.; Ailion, D. C.; Ganesan, K.; Laicher, G.; Goodrich, K. C.; Cutillo, A. G. *J. Magn. Reson. B* **1996**, *110*, 132–135.
(63) Nusser, W.; Kimmich, R.; Winter, F. *J. Phys. Chem.* **1988**, *92*, 6808–6814.
(64) Kimmich, R.; Nusser, W.; Gneiting, T. *Colloids Surf.* **1990**, *45*, 283–302.
(65) Zhang, C.; Tarhan, E.; Ramdas, A. K.; Weiner, A. M.; Durbin, S. M. *J. Phys. Chem. B* **2004**, *108*, 10077–10082.
(66) Xu, J.; Plaxco, K. W.; Allen, S. *J. Protein Sci.* **2006**, *15*, 1175–1181.
(67) Moritsugu, K.; Smith, J. C. *J. Phys. Chem. B* **2005**, *109*, 12182–12194.
(68) Balog, E.; Smith, J. C.; Perahia, D. *Phys. Chem. Chem. Phys.* **2006**, *8*, 5543–5548.

(69) Nederveen, A. J.; Bonvin, A. M. J. J. *J. Chem. Theory Comput.* **2005**, *1*, 363–374.

Both BPTI[70−72] and ubiquitin[73−75] have been subjected to several ^{15}N relaxation studies, yielding peptide N−H order parameters and effective correlation times for motions faster than the protein tumbling time of a few nanoseconds. The N−H groups that donate H-bonds to internal water molecules (Tyr10−W112 and Lys41−W113 in BPTI and Leu43−W28 in ubiquitin) have large orientational order parameters, consistent with the structure stabilizing role of these water molecules. The N−H order parameters derived from residual dipolar couplings are significantly smaller, as expected since they sample motions up to the millisecond range.[6] However, like the water ^{2}H and ^{17}O order parameters reported here, the peptide N−H order parameters are dominated by the most populated conformations in the equilibrium ensemble. The "open" conformations that allow internal water molecules to exchange are likely to be much more short-lived than the native "closed" conformation. These transient conformational states will therefore have too small equilibrium populations to be detected via order parameters. The very small equilibrium population of such high-energy conformational states also makes it difficult or impossible to detect them via the relaxation effects induced by the associated chemical shift changes. Such relaxation measurements have been used to monitor transitions among different conformers of the 14−38 disulfide bond in BPTI[76,77] and local conformational exchange processes of certain residues in ubiquitin.[78,79] However, these particular motions involve regions remote from the internal water molecules studied here and occur on much longer (millisecond) time scales than water exchange.

The primary role of the internal water molecules in BPTI and ubiquitin is probably to stabilize the native protein structure. In BPTI, W111−W113 connect the two extended loops that are involved in the recognition of and tight binding to β-trypsin.[19−22] In ubiquitin, W28 links the last residue (Leu50.O) of the β-sheet with the fourth β-strand (Leu43.N),[26−28] thereby stabilizing the nearby hydrophobic patch (centered around Ile44) that mediates interactions with many ubiquitin-binding domains.[81] While the internal water molecules in BPTI and ubiquitin may be indirectly linked to function, these proteins were chosen here to demonstrate the capabilities of the MRD/EMOR method. A variety of applications of this method to problems of high biological relevance can be envisaged. For example, water exchange, displacement or transport in connection with substrate binding or large-scale conformational transitions can be monitored in crosslinked or otherwise immobilized proteins of any size at physiological hydration levels. Membrane proteins, including aquaporins, can be studied in cubic phases, which like the present gels have the required spatial isotropy. If water molecules participate directly in the functional events, their residence times are crucial parameters. More generally, structural water molecules can be used to probe the dynamics of the large-scale conformational changes that govern their exchange rates.

5.3. Scope and Limitations. Here, we have determined residence times from 20 ns to 6 μs directly from the frequency dependence of R_1, but correlation times as long as 100 μs can be determined indirectly from the amplitude of the low-frequency plateau in the MRD profile (Figure 2). If a protein contains many internal water molecules, the individual contributions may not be separable in the MRD profile. However, difference-MRD experiments with protein mutants or water-displacing ligands can be used to assign residence times to unique hydration sites, as previously done in solution MRD studies.[17]

To isolate contributions from labile deuterons and as an additional check on the MRD/EMOR method, we recorded ^{17}O MRD profiles as well as ^{2}H profiles in this work. If the labile deuteron contribution can be excluded or controlled, ^{2}H MRD is more generally useful owing to the wider range of accessible frequencies and motional time scales. In addition, by comparing ^{2}H MRD profiles at different pD values, it is possible to probe side-chain dynamics (section 4.3). Other crosslinking agents than glutaraldehyde can be used to allow pD variation over a wider range.

By comparing the ^{2}H and ^{17}O order parameters, it is usually possible to decide if an internal water molecule performs C_2 flips during its residence time.[17,35] If this is the case, then the direct relaxation contribution from the flip motion should be manifested in the ^{2}H MRD profile. The flip rate can thus be determined and used to characterize the underlying cavity fluctuations in much the same way as has been done for aromatic ring flips.[81]

In quantitative comparisons of ^{2}H and ^{17}O MRD profiles acquired on different samples, H/D isotope effects must be considered. As illustrated by the present results, residence times obtained from D_2O samples are generally longer than their H_2O counterparts because X−D⋯Y bonds are slightly stronger than X−H⋯Y bonds[82] and, possibly, because the protein is less flexible when dissolved in D_2O.[83] These complications can be avoided by recording the ^{2}H and ^{17}O MRD profiles from the same sample, prepared with ^{17}O-enriched D_2O.

Supporting Information Available: Experimental procedures, including protein expression, protein immobilization, relaxation measurements, and electron microscopy as well as more details about the validation of the EMOR/MRD method. This material is available free of charge via the Internet at http://pubs.acs.org.

JA0775873

(70) Smith, P. E.; van Schaik, R. C.; Szyperski, T.; Wüthrich, K.; van Gunsteren, W. F. *J. Mol. Biol.* **1995**, *246*, 356−365.
(71) Beeser, S. A.; Oas, T. G.; Goldenberg, D. P. *J. Mol. Biol.* **1998**, *284*, 1581−1596.
(72) Sareth, S.; Li, H.; Yamada, H.; Woodward, C. K.; Akasaka, K. *FEBS Lett.* **2000**, *470*, 11−14.
(73) Schneider, D. M.; Dellwo, M. J.; Wand, A. J. *Biochemistry* **1992**, *31*, 3645−3652.
(74) Lienin, S. F.; Bremi, T.; Brutscher, B.; Brüschweiler, R.; Ernst, R. R. *J. Am. Chem. Soc.* **1998**, *120*, 9870−9879.
(75) Kitahara, R.; Yokoyama, S.; Akasaka, K. *J. Mol. Biol.* **2005**, *347*, 277−285.
(76) Otting, G.; Liepinsh, E.; Wüthrich, K. *Biochemistry* **1993**, *32*, 3571−3582.
(77) Grey, M. J.; Wang, C.; Palmer, A. G. *J. Am. Chem. Soc.* **2003**, *125*, 14324−14335.
(78) Dittmer, J.; Bodenhausen, G. *J. Am. Chem. Soc.* **2004**, *126*, 1314−1315.
(79) Massi, F.; Grey, M. J.; Palmer, A. G. *Protein Sci.* **2005**, *14*, 735−742.
(80) Hurley, J. H.; Lee, S.; Prag, G. *Biochem. J.* **2006**, *399*, 361−372.
(81) Hattori, M.; Li, H.; Yamada, H.; Akasaka, K.; Hengstenberg, W.; Gronwald, W.; Kalbitzer, H. R. *Protein Sci.* **2004**, *13*, 3104−3114.

(82) Scheiner, S. *Biochim. Biophys. Acta* **2000**, *1458*, 28−42.
(83) Cioni, P.; Strambini, G. B. *Biophys. J.* **2002**, *82*, 3246−3253.

Supporting Information

Nanosecond to microsecond protein dynamics probed by magnetic relaxation dispersion of buried water molecules

Erik Persson and Bertil Halle

Contribution from the Department of Biophysical Chemistry,
Center for Molecular Protein Science, Lund University, SE-22100 Lund, Sweden

Materials and Methods

Ubiquitin Expression and Purification. Ubiquitin was expressed in *E. coli* BL21 DE3 PLysS Star. Single colonies were used to inocculate overnight cultures of LB medium with 50 μg ml^{-1} ampicillin and 30 μg ml^{-1} chloramphenicol. These cultures were diluted 100-fold in the day cultures of 500 ml each in 2.5 L baffled flasks. Protein production was induced by adding 0.4 mM isopropyl-β-D-1-thiogalactosid at OD 0.6–0.8 (600 nm), and the cultures were harvested by centrifugation 3–4 h later. The pellet was resuspended in buffer A (20 mM NaAc, pH 5) and sonicated for 5 min, followed by centrifugation at 15000 rpm for 15 min. The supernatant was poured into an equal volume of boiling buffer A, heated to 80 ºC and then directly cooled on ice. The solution was centrifuged and the supernatant was transferred to a 160 ml SP-Sepharose Fast Flow column equilibrated with buffer A. The protein was eluted with a linear 0–400 mM NaCl gradient in buffer A. The fractions were checked on agarose and SDS-PAGE gels and the ones containing ubiquitin were pooled and lyophilized. The lyophilized protein was resuspended in 15 ml H$_2$O and transferred to a Sephadex G50 gel filtration column with a bed volume of 1800 ml

(Sigma-Aldrich, St Louis, MO). The fractions were again checked on agarose and SDS-PAGE gels and the ones containing ubiquitin were pooled and lyophilized. This preparation was resuspended in 10 ml H_2O and desalted on a Sephadex G25 superfine gel filtration column (Sigma-Aldrich, St Louis, MO) in water. A final SDS-PAGE gel indicated >99% purity.

Protein Immobilization. Lyophilized protein was dissolved in D_2O (99.9 atom % ^2H, low paramagnetic content) from Cambridge Isotope Laboratories (Andover, MA) or in $H_2^{17}O$ (21.2% ^{17}O, 5.5% ^{18}O, lot I1-7317) from Cambridge Isotope Laboratories (Andover, MA). pH was adjusted by µl additions of HCl or NaOH followed by centrifugation at 15000 rpm for 3 min. For the sample at pD 6.5, the protein was dissolved in 75 mM PIPES buffer in D_2O (piperazine-N-N'-bis[2-ethane-sulfonic acid], lot 26F-5630) from Sigma-Aldrich (St Louis, MO). The protein concentration of the solution (before crosslinking) was determined by complete amino acid analysis (performed at the Amino Acid Analysis Center, Dept. of Biochemistry and Organic Chemistry, Uppsala University, Sweden) or spectrophotometrically (Shimadzu UV-1601) at 280 nm using a calibrated extinction coefficient.

The protein was crosslinked by addition of ice-cold 25% glutaraldehyde (GA) solution (MP Biomedicals Inc, Solon, OH, lot 5141H) to the protein solution at 6 ºC. After 1 min of vortexing, the solution was split in two: one part was transferred to a 10 mm o.d. NMR tube and allowed to polymerize overnight at 6 ºC and the second part was used for pH determination by letting the solution polymerize around the pH electrode. For D_2O gels, we report pD = pH* + 0.41, where pH* is the operational pH (not corrected for H/D isotope effects). The BPTI gels had a yellowish translucent appearance, whereas the ubiquitin gels were opaque.

Magnetic Relaxation Dispersion. The longitudinal relaxation rate, R_1, of the water ^2H magnetization was measured over five frequency decades, from 1.5 kHz to 92 MHz. To cover

this frequency range, we used six different NMR instruments: a Stelar Spinmaster 1 Tesla fast field-cycling (FC) spectrometer (1.5 kHz – 6.4 MHz); a Tecmag Discovery spectrometer equipped with an iron-core magnet (Drusch EAR-35N), variable-field lock and flux stabilizer (11.7 MHz); and four spectrometers equipped with conventional cryomagnets: Bruker Avance DMX 100 (15.4 MHz), Varian Unity Plus 400 operated at 55.5 MHz, Varian Unity Inova 500 (76.8 MHz), and Varian Unity Inova 600 (92.1 MHz).

The longitudinal, R_1, and transverse, R_2, relaxation rates of the water ^{17}O magnetization were measured over 2.5 frequency decades, using Tecmag spectrometers equipped with iron-core magnets from GMW Associates (San Carlos, CA) (0.5 – 1.7 MHz) or Drusch (2.2 – 10.5 MHz) and conventional spectrometers with cryomagnets (13.6, 27.1, 48.5, 67.8 and 81.3 MHz).

For FC measurements, the pre-polarized (PP) and non-polarized (NP) sequences were used with polarization at 6.14 MHz (for PP) and detection at 4.80 MHz. The polarization and recovery times were set to 4 times T_1. In the non-FC experiments, standard inversion recovery (R_1) or spin echo (R_2) pulse sequences were used. Single-exponential recovery/decay curves were obtained throughout, from which the relaxation rate was determined by a 3-parameter fit. The estimated experimental error in R_1 is less than 1.5%. The sample temperature was maintained at 20.0 ± 0.1 °C by a thermostated air flow and was checked before and after each relaxation time measurement with a thermocouple referenced to an ice-water bath. The ^{2}H and ^{17}O relaxation rates of pure water reference samples with the same isotope composition as in the protein gels were also measured at 20 °C, yielding $R_{1,\text{bulk}} = 2.61$ s^{-1} (^{2}H) and 159.9 s^{-1} (^{17}O).

Fits to the MRD data were made with the Levenberg-Marquardt nonlinear least-squares algorithm with equal weighting of all data points. Quoted uncertainties in parameter values (one

standard deviation) are based on an estimated 1.5 % accuracy in all R_1 values. The target function for the fit was Eq. 1.

Electron Microscopy. Gels cut in ~1 mm cubes were immersed in 0.1 M potassium phosphate buffer containing 2% OsO_4 and were then rinsed 3×10 min in distilled H_2O. The gel cubes, immersed in distilled H_2O containing 2% uranyl acetate, were then kept in the dark for 1 h, followed by 3×10 min rinsing in distilled H_2O. The samples were stored at 4 °C overnight. Next, the gel cubes were immersed in acidic DMP (dimethoxypropane) for 20 min, followed by 2×10 min incubation in acetone. The samples were then infiltrated with Spurr's resin: 75% acetone : 25% resin (20 min), 50% acetone : 50% resin (20 min), 25% acetone: 75% resin (20 min) and 100% resin (1.5 h), followed by an incubation with 100% resin (1.7 h) without lid. All the infiltration steps were performed on a rotator. Samples in 100% resin contained in capsules were placed in an oven at 70 °C for 16 h. The resulting resin blocks were trimmed with blades and thin-sectioned. Thin sections were collected on formvar coated copper grids and stained with Reynold's lead citrate for 4 min. Sections on the grid were washed in distilled H_2O, air-dried and examined at 120 kV on a Philips CM120 BioTWIN transmission electron microscope.

Results and Discussion

Validation of the EMOR/MRD Method. Figure S1 shows ^{2}H MRD profiles from BPTI immobilized under different conditions. The figure includes the previously discussed profiles at pD 4.4 and 6.5, which coincide above ~ 10 MHz but differ by 9% at low frequencies. As discussed in Sect. 4.3, this small difference results from a COOD contribution at pD 4.4. The remaining two MRD profiles in Fig. S1 were also recorded at pD 4.4 ± 0.1, but with higher protein or GA concentration (Table 1).

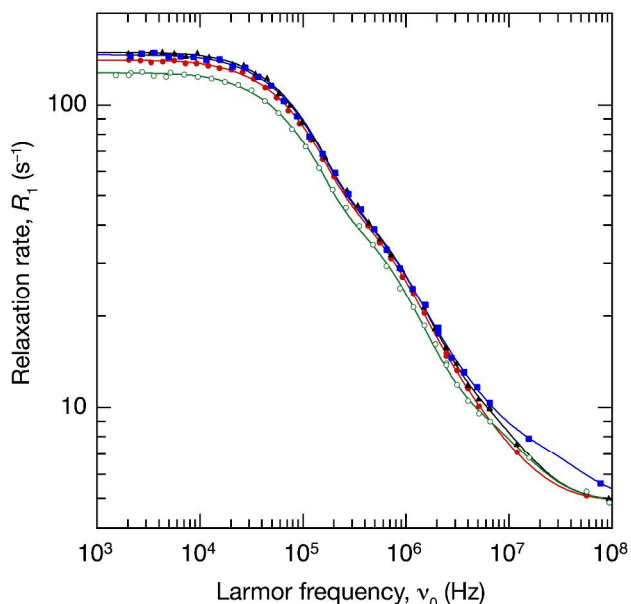**Figure S1.** Water ^{2}H MRD profiles from immobilized BPTI at 20 °C. The data were measured on samples B2 (green, ○), B3 (red, ●), B4 (black, ▲) and B5 (blue, ■) and are normalized to $N_W = 3000$. The solid curves were obtained by fitting the model to the R_1 data as in Fig. 3a. Note the logarithmic R_1 scale.

Decreasing the water/BPTI mole ratio, N_W, by 36% (sample B3 → B4) increases the N_W-normalized R_1 by 6% at the lowest frequency, but has little or no effect above 10 MHz. Increasing the GA/protein mole ratio, N_{GA}, by 72% (sample B3 → B5) increases the N_W-normalized R_1 by 4% at the lowest frequency. Since sample B5 had a protein concentration intermediate between samples B3 and B4, the cause of this R_1 increase may be the higher protein concentration rather than more extensive crosslinking. More significantly, above 10 MHz the excess relaxation rate, $R_{1,ex}$, is up to 25% higher in sample B5 than in the other samples. A plausible explanation of this observation is that a higher crosslinker concentration leads to more extensive protein clustering, manifested in a larger amplitude of the slow surface hydration component.

The universal nanosecond dispersion component, which we tentatively attribute to overlapping hydration layers, might also be produced by the internal water molecules in a fraction, x_0, of non-crosslinked, freely tumbling protein molecules. For this fraction, the relaxation mechanism would then be the same as in solution. However, several facts argue against this possibility. First, the high N_{GA} sample B5 should have a lower fraction, x_0, but the nanosecond component has larger amplitude in this sample (Fig. S1). Second, BPTI has more internal water than ubiquitin and should therefore have a much larger amplitude parameter than ubiquitin, whereas, in fact, $N_S^{slow}(S_S^{slow})^2$ is slightly smaller for BPTI. Third, the ^{17}O amplitude parameter, $N_S^{slow}(S_S^{slow})^2$, for ubiquitin would in this interpretation be $x_0 S_{W28}^2 < 0.35$ (Table 3), an order of magnitude smaller than observed. In summary, the results in Fig. S1 demonstrate that the protein dynamics that govern internal water exchange are essentially unaffected by substantial variations in protein and crosslinker concentrations

We have tacitly assumed that the crosslinked protein molecules are completely immobilized. But if the crosslinks are flexible, the protein might still undergo rotational diffusion of restricted angular amplitude. This would have two consequences. First, the order parameter in the EMOR mechanism is not the internal order parameter, S_k, but the product $S_k S_{RRD}$, where the order parameter S_{RRD} is determined by the amplitude of restricted rotational diffusion (RRD). Second, the RRD motion would give a direct contribution to R_1 with a correlation time of order τ_{RP} or shorter. Could this be the origin of the universal nanosecond dispersion component? Because the amplitude parameter $N_S^{slow}(S_S^{slow})^2$ would then be given by $(1 - S_{RRD}^2)\sum_k N_k S_k^2$, it should by larger for BPTI than for ubiquitin (since BPTI has more internal water) and it should be larger for ^2H than for ^{17}O (since W112 and W133 hardly contribute to the ^{17}O MRD profile). Neither of these predictions agrees with the experimental data. Furthermore, the ^{17}O amplitude parameter $N_S^{slow}(S_S^{slow})^2$ for ubiquitin should be < 0.35 (Table 3), whereas, in fact, it is 4 ± 2. Therefore, gel flexibility cannot explain the nanosecond dispersion component.

The quantitative agreement between predicted and measured effective amplitude parameters (Table 4) suggests that the crosslinked proteins are, in fact, highly immobilized, with S_{RRD} close to 1. For example, with $S_{RRD} = 0.7$, the predicted amplitude parameters would have been only half of the measured ones.